



## Combined Upper Limit on Standard Model Higgs Boson Production for Summer 2009

The CDF Collaboration  
URL <http://www-cdf.fnal.gov>  
(Dated: August 26, 2009)

This note describes a combination of searches for the Standard Model Higgs boson at CDF. The six major analyses combined are the  $WH \rightarrow \ell\nu b\bar{b}$  channels, the  $WH + ZH \rightarrow \cancel{E}_T + b\bar{b}$  channels, the  $ZH \rightarrow \ell^+\ell^- b\bar{b}$  channels, the  $H \rightarrow \tau^+\tau^-$  channel, the  $WH + ZH \rightarrow jj + b\bar{b}$  channel, and the  $H \rightarrow W^+W^- \rightarrow \ell^+\nu_\ell\ell'^-\bar{\nu}_{\ell'}$  opposite-sign channels and the  $WH \rightarrow WW^+W^-$  same-sign dilepton channel. The integrated luminosity for the channels varies between  $2.0 \text{ fb}^{-1}$  and  $4.8 \text{ fb}^{-1}$ . The 95% CL upper limit on  $R = \sigma_H/\sigma_{H,SM}$  is computed as a function of  $m_H$  from 100 to 200  $\text{GeV}/c^2$  in steps of  $5 \text{ GeV}/c^2$ , assuming Standard Model decay branching fractions of the Higgs boson and that the ratios of the rates for the  $WH$ ,  $ZH$ ,  $gg \rightarrow H$  and vector-boson fusion  $qq \rightarrow Hqq$  production mechanisms are those predicted by the Standard Model. The results are in good agreement with those expected in the background-only hypothesis, and the observed (expected) limits on  $R$  are 3.62 (2.53) and 1.24 (1.29) at Higgs boson masses of 115 and 160  $\text{GeV}/c^2$ , respectively.

*Preliminary Results for Summer 2009 Conferences*

## I. INTRODUCTION

A combination of the different Higgs search analysis results provides many advantages. Since the decay branching ratios of the Standard Model (SM) Higgs boson are strong functions of its mass  $m_H$ , the different search channels contribute in a complementary way to the sensitivity at different  $m_H$ . Some analyses seek the Higgs boson in the same decay mode but with different production mechanisms, and hence require separate treatments of the signals and backgrounds. Since these analyses all seek the same particle, the best results are obtained by combining the searches together.

A previous combination [1] has been performed using the results of the six main searches for the Standard Model Higgs boson at CDF, the  $WH \rightarrow \ell\nu b\bar{b}$  channels, the  $WH + ZH \rightarrow \cancel{E}_T + b\bar{b}$  channels, the  $ZH \rightarrow \ell^+\ell^-b\bar{b}$  channels, the  $H \rightarrow \tau^+\tau^-$  channel, the  $H \rightarrow W^+W^- \rightarrow \ell^+\nu_\ell\ell'^-\bar{\nu}_{\ell'}$  channels, and the  $WH + ZH \rightarrow jjb\bar{b}$  channel. This note presents an update of the combination, using newly released results for the  $H \rightarrow W^+W^- \rightarrow \ell^+\nu_\ell\ell'^-\bar{\nu}_{\ell'}$  opposite-sign and same-sign dilepton channels, as well as introducing a new low- $m_{\ell\ell}$  channel. The  $WH \rightarrow \ell\nu b\bar{b}$  channels are updated to  $4.3 \text{ fb}^{-1}$ , using a neural-network analysis technique. The  $WH + ZH \rightarrow \cancel{E}_T + b\bar{b}$  channels are updated to include  $3.6 \text{ fb}^{-1}$  of data, and the  $ZH \rightarrow \ell^+\ell^-b\bar{b}$  channels are updated to include  $4.1 \text{ fb}^{-1}$  of data. The  $H \rightarrow \tau^+\tau^-$  and  $WH + ZH \rightarrow jjb\bar{b}$  channels remain unchanged since [1]. The analyzed luminosities and references to the documentation are provided in Table I.

In order to combine the results of the six search analyses, assumptions must be made about the model to be tested. The model tested by the individual analyses' notes is a model in which Standard Model Higgs boson production proceeds, but is enhanced, in all production mechanisms, by a factor of  $R$  in the cross section. The decay branching fractions and the width of the invariant mass distribution of the Higgs boson are assumed to be those predicted by the Standard Model. Exotic models which change the Higgs boson production cross section may not follow this pattern. If a fourth generation of fermions exists, for example, it would enhance the  $gg \rightarrow H$  production cross section by a factor of roughly 9 [8], but would not enhance the  $WH$  and  $ZH$  associated production mechanisms. A heavy neutrino in the fourth generation may take some of the Higgs boson decay branching ratio if it is light enough for the Higgs boson to decay into. The Standard Model production cross sections and decay branching ratios used in this combination are the same as those used in the previous combination [1]. In particular, the  $gg \rightarrow H$  production cross section is calculated at NNLL in QCD and also includes two-loop electroweak effects [9, 10]. The  $gg \rightarrow H$  production cross section depends strongly on the PDF set chosen and the accompanying value of  $\alpha_s$ . These calculations use the MSTW 2008 NNLO PDF set [11]. These supersede the cross sections used in the update of Summer 2008 [12, 13]. The newer cross sections include a more thorough treatment of higher-order radiative corrections, particularly those involving  $b$  quark loops, as well as using the MSTW 2008 PDF set instead of the MRST 2002 PDF set [14]. The Higgs boson production cross sections used here are listed in Table II [10].

It has been pointed out [15] that the uncertainties in the  $gg \rightarrow H$  production cross section have been underestimated in the past, particularly if an experimental analysis separates data based on the number of jets produced in association with the Higgs boson. We have updated the uncertainties in the  $gg \rightarrow H$  production cross section to include the scale uncertainties separately for each jet category (0, 1, and 2+ jets), and to separate out also the PDF uncertainty in the production cross section as a separate source of uncertainty correlated across all  $gg \rightarrow H$  signal contributions. These uncertainties are used in the  $H \rightarrow W^+W^- \rightarrow \ell^+\nu_\ell\ell'^-\bar{\nu}_{\ell'}$  channels and also the  $H \rightarrow \tau^+\tau^-$  channel.

The cross sections listed in [12] for the  $WH$ ,  $ZH$  and  $VBF$  processes are on a coarser mass grid than desired, and so MCFM [16] has been used to compute the remaining required cross sections, and has been found to agree well with those in [12]. The decay branching ratios are computed with HDECAY [17].

Several updates and improvements have been made to the channels since the previous combination [1], and are listed below, in addition to the larger datasets that are analyzed.

- A new low- $m_{\ell+\ell^-}$  channel is added to the suite of  $H \rightarrow W^+W^- \rightarrow \ell^+\nu_\ell\ell'^-\bar{\nu}_{\ell'}$  channels, selecting events with  $m_{\ell+\ell^-} < 16 \text{ GeV}$ .
- A likelihood-based electron identification is added to the  $H \rightarrow W^+W^- \rightarrow \ell^+\nu_\ell\ell'^-\bar{\nu}_{\ell'}$  channels.
- Tighter control over  $W\gamma$  background is achieved in the  $H \rightarrow W^+W^- \rightarrow \ell^+\nu_\ell\ell'^-\bar{\nu}_{\ell'}$  through the use of the low- $m_{\ell\ell}$  same-sign control region.
- The  $WH \rightarrow \ell\nu b\bar{b}$  channels add a new loose double-tag category. This new category uses events with one tight SECVTX tag, and one jet tagged with a looser neural-network tag (ROMA).
- The  $WH \rightarrow \ell\nu b\bar{b}$  channels now include data from an inclusive MET trigger (MET45/MET40), to gain acceptance for the isolated-track channels.
- The  $WH \rightarrow \ell\nu b\bar{b}$  channels now use a neural-network-based b-jet energy correction

- The discriminant in the  $WH \rightarrow \ell\nu b\bar{b}$  channels now uses a Bayesian Neural Network.
- The  $WH + ZH \rightarrow \cancel{E}_T + b\bar{b}$  channels have updated the data-derived tag rate function and the QCD multijet scale factor to include new data.

The mass grid for the  $H \rightarrow W^+W^- \rightarrow \ell^+\nu_\ell\ell'^-\bar{\nu}_{\ell'}$  channels is in  $5 \text{ GeV}/c^2$  steps between  $m_H = 140 \text{ GeV}/c^2$  and  $180 \text{ GeV}/c^2$ , and in  $10 \text{ GeV}/c^2$  steps outside that interval. As the combination requires a  $5 \text{ GeV}/c^2$  step everywhere, the results have been interpolated for the test mass points 100, 105, 115, 125, and  $135 \text{ GeV}/c^2$  by starting the signal, background and data histograms from the nearest supplied point with a test mass heavier than the one desired. The signal histograms (separately supplied for each of the four signal processes) are then scaled by the ratios of the production cross section and the decay branching ratio for  $H \rightarrow W^+W^-$ , and a separate two-loop EW correction is applied. This method is approximate because it does not interpolate the acceptance. Results at  $m_H = 185$  and  $195 \text{ GeV}/c^2$  are not quoted here since the  $H \rightarrow W^+W^- \rightarrow \ell^+\nu_\ell\ell'^-\bar{\nu}_{\ell'}$  channels are the only ones to contribute, and these mass points were not included in the search. For the lower mass points, the  $H \rightarrow b\bar{b}$  searches dominate the sensitivity. The same interpolation scheme is applied to the  $H \rightarrow \tau^+\tau^-$  channel for the missing points at 125, 135, and  $145 \text{ GeV}/c^2$ .

## II. COMBINATION METHOD

A Bayesian technique is used to compute the observed and expected upper limits on  $R$ . The prior is flat in the product of  $R$  and the total expected signal yield after all efficiencies and acceptances are taken into account. This prior was used in the previous combination [1].

### A. Common Parameter Alignment

The individual channel analyses listed above require theoretical input in the form of kinematic distributions from Monte Carlo (usually from leading-order generators with parton shower models), and higher-order predictions of inclusive cross sections. The method of inclusion of systematic uncertainties, described below, takes advantage of shared dependence on common parameters, such as the luminosity, the  $t\bar{t}$  and single-top cross sections, the diboson cross sections and the vector-boson-plus-heavy-flavor-jets  $K$  factor relative to the Monte Carlo prediction.

Some of the individual analyses use an older prediction of the  $t\bar{t}$  cross section,  $6.7 \text{ pb}$  [18], assuming  $m_t = 175 \text{ GeV}/c^2$ . The analyses also use single top theoretical predictions [19] evaluated at  $m_t = 175 \text{ GeV}/c^2$ ,  $\sigma_s = 0.88 \text{ pb}$  for the  $s$ -channel production, and  $\sigma_t = 1.96 \text{ pb}$  for  $t$ -channel production. In discussions with D0, we choose to shift  $\sigma_{t\bar{t}}$  to its value at  $m_t = 172.4 \pm 1.2 \text{ GeV}/c^2$  [20], and to use newer, higher-order calculations [21]. The channels' background templates are evaluated with  $m_t = 175 \text{ GeV}/c^2$ , but since the kinematics are not expected to be strongly dependent on  $m_t$ , particularly in advanced discriminants designed to separate Higgs boson events from backgrounds, only the cross section has been adjusted. We use a value of  $\sigma_{t\bar{t}} = 7.794 \text{ pb}$ , with an uncertainty of 3.9% due to the uncertainty on  $m_t$ , 5.3% due to the factorization and renormalization scale, and 2.9% from PDF uncertainty. The single top cross sections [22] are, for the  $s$ -channel,  $1.083 \text{ pb} \pm 3.2\% (m_t) \pm 3.7\% (\text{scale}) \pm 1.9\% (\text{PDF})$ , and for the  $t$ -channel,  $2.295 \text{ pb} \pm 1.9\% (m_t) \pm 1.3\% (\text{scale}) \pm 5.2\% (\text{PDF})$ . The templates from each channel have been scaled by the appropriate ratios of cross sections to unify the predictions. The above theoretical uncertainties are applied in place of those supplied by the analyses. The scale and PDF uncertainties are taken to be uncorrelated between the three processes.

The  $W, Z$ +heavy-flavor  $K$ -factors are correlated between the  $WH \rightarrow \ell\nu b\bar{b}$  and the  $ZH \rightarrow \ell^+\ell^-b\bar{b}$  channels, but these are considered uncorrelated with the  $WH + ZH \rightarrow \cancel{E}_T + b\bar{b}$  channels, as the former use ALPGEN [23] to model  $W, Z$ +heavy-flavor events, and the latter use Pythia [24]. This decorrelation is conservative since the common handling of shared systematic uncertainties allows one channel's data to constrain another channel's background, and if the  $K$ -factors or other central values are not aligned, sharing a common uncertainty is an aggressive procedure.

The diboson processes  $WW$ ,  $WZ$  and  $ZZ$  have been assigned a common theoretical uncertainty of 11.5%, shared across all channels.

The signal cross section uncertainties [12] have been unified across channels. We assign separate scale and PDF uncertainties for  $gg \rightarrow H$  production, in a jet-bin-dependent way, correlating the uncertainties across jet bins [15]. We assume a 5% uncertainty on  $WH$  and  $ZH$  production (correlated between  $WH$  and  $ZH$ ), and a 10% uncertainty on vector-boson fusion, both independent of  $m_H$ . The theoretical uncertainties on the separate Higgs boson production mechanisms are considered to be independent of each other and of all other uncertainties.

The luminosity uncertainties are split into a ‘‘Luminosity’’ category which refers to our uncertainty on the inelastic  $p\bar{p}$  cross-section, and a ‘‘Luminosity Monitor’’ category, which refers to CDF-specific luminosity uncertainty. The

“Luminosity” category, taken to be 3.8% and the “Luminosity Monitor” uncertainty is taken to be 4.4% for all templates of signal and background that are normalized to theoretical predictions times the luminosity measurement. Components that are already normalized to data observations in control samples do not have this uncertainty. This breakdown is necessary for proper correlation with D0’s luminosity uncertainty.

## B. Systematic Uncertainties

Systematic uncertainties are incorporated by marginalizing the likelihood function over variations in the uncertain parameters, called “nuisance parameters”. Each nuisance parameter is considered to be independent of the others, but each one may have an effect on any of the signal or background predictions in any of the channels. Nuisance parameters included in this combination include the integrated luminosity, the jet energy scale, the b-tag efficiency scale factor, mistag uncertainties, the lepton trigger efficiencies, the lepton identification efficiencies and fake rates, Monte Carlo generator differences, uncertainties due to missing higher-order terms in the signal and background MC predictions, Monte Carlo modeling of ISR, FSR and PDFs, background production cross sections for  $t\bar{t}$ , diboson, and other backgrounds, mistag matrix uncertainties, the heavy-flavor fraction in  $W$ +jets, and the uncertainties in non- $W$  contributions. Full listings of the nuisance parameters affecting these analyses are summarized in tables for each channel at the end of this note. The nuisance parameters affect the predicted rates of different signal and background processes, and some nuisance parameters have shape uncertainties associated with them as well.

Rate uncertainties on template histograms are incorporated by multiplying the dependences of each rate on each nuisance parameter.

$$s_{\text{varied}} = s_{\text{central}} \prod_{i=1}^{n_{\text{params}}} (1 + f_i \eta_i) \quad (1)$$

where  $s_{\text{varied}}$  is the systematically varied normalization scale factor on a particular prediction histogram (signal or background) in a channel,  $s_{\text{central}}$  is the central-value normalization scale factor for that template,  $f_i$  is the relative uncertainty on  $s$  due to nuisance parameter  $i$ , and  $\eta_i$  is the random truncated-Gaussian-distributed nuisance parameter. Indices for the analysis channel and background or signal source template have been suppressed. The multiplicative technique used here means that the nuisance parameter truncations are all independent of each other.

Shape uncertainties are handled by varying the template shapes according to the nuisance parameters  $\eta_i$ . Systematically-varied shapes are supplied by the analysis teams as histograms which are generated with systematically varied parameters. These parameters may be the same ones as are responsible for the rate variations, and the variations are taken to be correlated. For example, a jet energy scale variation affects both the rate and the shape of most expected signal histograms. All analyses now use histograms of sophisticated multivariate discriminants in order to present their results, and the left-right template shifting interpolation is no longer used to incorporate shape uncertainties. Instead, the simpler method of linearly interpolating between the central value shapes and the systematically varied shapes in each bin according to the value of the nuisance parameter. Shape systematics are compounded by adding linearly the changes due to several shape variations in each bin. Shape systematics are extrapolated beyond the usual  $\pm 1\sigma$  variations provided by the analysis teams. If a particular choice of shape variations results in a negative prediction for any signal or background component in any bin, then the prediction for that component is set to zero in that bin, but it does not prevent that variation from being applied to other bins. It is recommended that in the future analyzers investigate what multi-sigma variations in systematic parameters do to the predicted final discriminant shapes.

Another source of rate and shape variation is limited MC statistics in each bin of the template histograms. Each analysis supplies histograms along with their independent uncertainties in ROOT histogram objects. These uncertainties do not include the correlated rate and shape uncertainties described above, but are meant to cover the effects of MC statistics (or data statistics, if data control regions are used to predict the composition of the selected events in the signal region).

## C. Numerical Integration

The space spanned by the nuisance parameters has a very large dimension – 59 uncertain parameters in all at  $m_H = 115$  GeV, and 30 parameters at  $m_H = 160$  GeV. The posterior calculation integrates over all possible values of the nuisance parameters, weighted by their priors. In the combination of Summer 2008 [25], the the nuisance parameter marginalization is done by random Monte Carlo integration. Points within the nuisance parameter space are selected randomly using truncated Gaussian distributions with unit width (before truncation). The domain of

each nuisance parameter is truncated in order to keep the prediction of the rate of each template non-negative; no other truncation is applied. Since analyzers supply  $\pm 1\sigma$  uncertainties on rates and shapes, the impacts of multi-sigma variations are extrapolations of the one sigma variations.

The number of nuisance parameters increases as more search channels are added, and the gap between the prior information about a nuisance parameter and what can be determined from the data about a particular nuisance parameter has been increasing as well, for certain key nuisance parameters. For example, the  $W, Z$ +Heavy Flavor rate has an uncertainty of  $\sim 40\%$ , mainly by fitting heavy-flavor fractions to control samples in the data that do not overlap with the  $W, Z$ +2-jet samples used for the signal extraction. But large amounts of data in the  $W, Z$ +2-jet samples have been accumulated, and these constrain the  $W, Z$ +Heavy Flavor rate much more precisely than the priors – by approximately a factor of five. This has a large effect on the random-sampling integration method because most samplings of the  $W, Z$ +Heavy Flavor rate parameter produce predictions that are at large variance with the data observations, and result in very small values of the likelihood, and contribute very little to the integral. One or two such parameters do not present a computational challenge, but the presence of many such parameters has the effect that nearly all samples of the systematic errors contribute very little, and one or two samples in a large run will contribute nearly all of the weight of the integral.

A new approach has been taken to perform the integrals over the nuisance parameters, that of Markov Chain Monte Carlo integration. The Metropolis-Hastings algorithm [26] is used. This algorithm has found broad use in high-dimensional integrals elsewhere, particularly in the application of Bayesian statistics. All integrals start at the point in nuisance parameter space at which all parameters are zero (corresponding to the central values of all predictions). A proposal function determines where to step next in nuisance parameter space, and the Markov Chain moves to the proposed point if it has a higher value of the likelihood or if a random number between 0 and 1 is less than the ratio of the likelihood at the new point divided by the likelihood at the old point. This algorithm focuses on parts of parameter space for which the integrand is largest, thus saving computational resources and producing more reliable results in shorter times.

We use the Markov Chain Monte Carlo integration technique for  $m_H \leq 150$  GeV, where the low-mass  $H \rightarrow b\bar{b}$  channels contribute. For the high-mass range, we revert to the random Monte Carlo integration technique, which still produces reliable results for the channels there.

All limits are quoted at the 95% credibility level. Expected limits are computed using a sample (1000) of background-only pseudoexperiments for each mass point of each analysis or combination. On each pseudoexperiment, new values of the nuisance parameters are drawn from the Gaussian distributions specified in the systematic uncertainty tables, and Poisson random pseudodata are drawn from the systematically smeared predictions. In order to reduce the amount of CPU used in the combination and to get more reliable  $\pm 2\sigma$  expected limit estimations, the distribution of limits in the pseudoexperiments is fit to the density function  $d(R)$ :

$$d(R) = p_1(R - p_2)^{p_3} e^{-p_4 R}, \quad (2)$$

where  $p_1, p_2, p_3$ , and  $p_4$  are freely-floating fit parameters. This function is then integrated to obtain the desired quantiles, which correspond to 2.275% of limits being below the  $-2\sigma$  limit expectation in a large ensemble of background-only outcomes, 16% being below the  $-1\sigma$  limit expectation, 50% being below the median expectation, 84% being below the  $+1\sigma$  expectation, and 97.725% being below the  $+2\sigma$  expectation.

### III. INDIVIDUAL CHANNEL LIMITS

In order to validate the input histogram preparation and the combination method, the observed and expected limits have been recomputed for each of the contributing channels before the final combination is performed. The rates and systematic uncertainties of each of the signal contributions and the backgrounds are compared with the available documentation. For the individual channel limits, the same Markov Chain integration technique is performed as for the combination, and the numerical precision due to Monte Carlo statistics in the limit calculation and the expected limit calculation is expected to be below 2%. Tables at the end of this note compare the observed and expected limits blessed by the analysis teams and the reproductions computed here. In most cases, the agreement is exquisite, since the same programs are used to compute the individual limits as is used to combine many channels together. Some channels use different software packages however and the agreement is within 10%.

### IV. COMBINATION RESULTS

The results of the combination are given in Table XVII, and in Figure 1. Figure 2 compares the observed and expected limits obtained in combination with those of the individual analyses. The SM Higgs mass limit from

LEP [27] is included in the plots. The same procedure for computing the individual channel limits is applied, but a joint likelihood is formed for all channels together, and variations of shared nuisance parameters, which affect both rates and shapes, are all performed with 100% correlations between parameters with the same name, and 0% correlation between parameters with different names.

The posterior of the combined results is shown in Figures 3 and 4 for each value of  $m_H$  between 100 and 200  $\text{GeV}/c^2$  in 5  $\text{GeV}/c^2$  steps. The distributions of the limits expected in background-only pseudoexperiments are shown in Figures 5 and 6.

To visualize the combined results better, the data are collected from all channels and are classified by the signal-to-background ratio in each bin. Bins of nearby  $s/b$  are collected together, and plotted vs  $\log_{10}(s/b)$  in Figures 7 for  $m_H = 115$  and  $160 \text{ GeV}/c^2$ . The data are then integrated from the high  $s/b$  side towards the lower, and the data counts are shown in Figure 7 for the same two Higgs boson masses. These integrals answer the question of how many events were observed, compared with the signal and background predictions. Because many bins of different  $s/b$  are used to make the final limit, there is an arbitrary choice of where to put a cut to answer that question. Figure 7 shows that answer for several high- $s/b$  cuts. Drawbacks of this representation are that systematic uncertainties are not shown.

## V. PROJECTIONS

As data are accumulated, the sensitivity of the searches is expected to increase. A naive extrapolation of the sensitivity is to scale the median expected limit with  $1/\sqrt{\int L dt}$ . This approximation makes several assumptions: 1) that the background levels in the high  $s/b$  bins is sufficiently large that the distribution of data events is expected to be in the Gaussian regime of the Poisson distribution, 2) that the systematic uncertainties scale with  $1/\sqrt{\int L dt}$  for each channel, 3) that the analysis techniques remain constant, 4) that the detector performance remains constant and also does not degrade with increased instantaneous luminosity, and 5) that the tested models do not change. The experience on CDF is that the detector performance remains nearly constant, with only a mild drop due to the increased instantaneous luminosity. Larger control samples allow better constraints on systematic uncertainties, and also can be used to test extrapolations into signal regions by refining the definitions of the control samples. Analysis improvements such as increasing acceptance by exploiting previously unused trigger paths and event topologies, as well as improved separation of signal from background through the use of multivariate techniques and combinations of multivariate techniques have brought about increases in sensitivity that surpass what is expected from the  $1/\sqrt{\int L dt}$  dependence alone. The comparison of the achieved expected limits and the  $1/\sqrt{\int L dt}$  extrapolations is shown in Figure 8 for  $m_H = 115$  and  $160 \text{ GeV}/c^2$ .

In Figure 8, the integrated luminosity at which to place a point is a simple weighted average of the contributing analyses' integrated luminosities. The  $WH \rightarrow \ell\nu b\bar{b}$  and  $WH + ZH \rightarrow \cancel{E}_T + b\bar{b}$  are given twice the weight of the  $ZH \rightarrow \ell^+\ell^-b\bar{b}$  channel and four times the weight of the  $H \rightarrow \tau^+\tau^-$  and  $WH + ZH \rightarrow jjb\bar{b}$  channels, for the  $m_H = 115 \text{ GeV}$  point.  $m_H = 160 \text{ GeV}/c^2$  points, only the  $H \rightarrow W^+W^- \rightarrow \ell^+\nu_\ell\ell'^-\bar{\nu}_{\ell'}$  channels' luminosity ( $4.8 \text{ fb}^{-1}$ ) is used. In the  $m_H = 160 \text{ GeV}/c^2$  plot, the limits from Summer 2004 and Summer 2005 have been scaled to use the NNLO  $gg \rightarrow H$  cross section which is approximately 50% larger than the NLO cross section, which was used in the original analyses. Only the ICHEP 2008 point includes the scaling using the new 2-loop electroweak diagrams, however.

The projection figures include estimations of how much the sensitivity could be improved over time as work is done on the analyses. The estimations were made in late 2007, based on the Summer 2007 estimations of sensitivity. A factor of 1.5 in the expected limit was estimated to be attainable with improvements known to exist but not yet in the analyses, and a further factor of 1.5 was estimated from ideas that had yet to be tried. Both of these curves are shown, as the top and bottom edges of light orange bands in the figures. For both the low-mass and high-mass searches, the first factor of 1.5 has already been achieved.

Figure 9 shows the same projections, but the expected limits have all been divided by  $\sqrt{2}$  to simulate the effect of combining with D0, assuming performance equal to CDF's. Figure 10 shows the chances of observing a  $2\sigma$  excess or  $3\sigma$  evidence as a function of  $m_H$ , assuming a Higgs boson is present and the production cross section and decay parameters are as predicted by the SM. CDF and D0 are assumed to contribute equally, and the performance level is shown both for the currently achieved performance level and also for an additional factor of 1.5. Two luminosity scenarios are considered,  $5 \text{ fb}^{-1}$  and  $10 \text{ fb}^{-1}$  of analyzed luminosity per experiment. Only the sensitivity estimated by the signal and background templates and their systematic uncertainties is shown in these plots, and no account is taken of the data already observed. In particular, a deficit in the Tevatron combination for  $m_H$  between 160 and

170 GeV/ $c^2$  allows the exclusion of that mass region [28], and so the chances of observing an excess or evidence are lessened when considering the data. Furthermore, even if a SM Higgs boson is nonetheless assumed to exist in that range, it will take more data and additional luck in order to accumulate enough candidates to amass the evidence after the unlucky downward fluctuation.

## VI. ACKNOWLEDGEMENTS

The authors would like to thank all members of the CDF Higgs Discovery group, particularly those who provided the results for combination.

- 
- [1] CDF Collaboration, CDF Note 9721 (2009).
  - [2] CDF Collaboration, CDF Note 9868 (2009).
  - [3] CDF Collaboration, CDF Note 9891 (2009).
  - [4] CDF Collaboration, CDF Note 9889 (2009).
  - [5] CDF Collaboration, CDF Note 9248 (2008).
  - [6] CDF Collaboration, CDF Note 9366 (2008).
  - [7] CDF Collaboration, CDF Note 9887 (2008).
  - [8] E. Arik, O. Cakir, S. A. Cetin and S. Sultansoy, *Acta Phys. Polon.* **B37**:2839-2850 (2006). Available online as [arXiv:hep-ph/0502050](https://arxiv.org/abs/hep-ph/0502050).
  - [9] C. Anastasiou, R. Boughezal and F. Petriello, "Mixed QCD-electroweak corrections to Higgs boson production in gluon fusion", [arXiv:0811.3458](https://arxiv.org/abs/0811.3458) [hep-ph] (2008).
  - [10] D. de Florian and M. Grazzini, "Higgs production through gluon fusion: updated cross sections at the Tevatron and the LHC", [arXiv:0901.2427v1](https://arxiv.org/abs/0901.2427v1) [hep-ph] (2009).
  - [11] A. D. Martin, W. J. Stirling, R. S. Thorne and G. Watt, "Parton distributions for the LHC, [arXiv:0901.0002](https://arxiv.org/abs/0901.0002) [hep-ph] (2009).
  - [12] TeV4LHC Higgs working group at <http://maltoni.home.cern.ch/maltoni/TeV4LHC/SM.html>.
  - [13] U. Aglietti, R. Bonciani, G. Degrassi, A. Vicini, "Two-loop electroweak corrections to Higgs production in proton-proton collisions", [arXiv:hep-ph/0610033v1](https://arxiv.org/abs/hep-ph/0610033v1) (2006).
  - [14] A. D. Martin, R. G. Roberts, W. J. Stirling and R. S. Thorne, *Phys. Lett. B* **531**, 216 (2002) [[arXiv:hep-ph/0201127](https://arxiv.org/abs/hep-ph/0201127)].
  - [15] C. Anastasiou, G. Dissertori, M. Grazzini, F. Stöckli and B. R. Webber, [arXiv:0905.3529](https://arxiv.org/abs/0905.3529) [hep-ph].
  - [16] J.M. Campbell, R.K. Ellis, *Phys. Rev. D* **62**:114012 (2000), [hep-ph/0006304](https://arxiv.org/abs/hep-ph/0006304). See also <http://mcfm.fnal.gov/index.html>.
  - [17] A. Djouadi, K.Kalinowski and M. Spira, *Comp. Phys. Commun.* **108C** 56 (1998).
  - [18] M. Cacciari, S. Frixione, M. L. Mangano, P. Nason and G. Ridolfi, *JHEP* **0809**, 127 (2008) [[arXiv:0804.2800](https://arxiv.org/abs/0804.2800) [hep-ph]].
  - [19] B. W. Harris, E. Laenen, L. Phaf, Z. Sullivan and S. Weinzierl, *Phys. Rev. D* **66**, 054024 (2002) [[arXiv:hep-ph/0207055](https://arxiv.org/abs/hep-ph/0207055)].
  - [20] The Tevatron Electroweak Working Group, for the CDF, D0 Collaborations, "Combination of CDF and D0 Results on the Mass of the Top Quark", [arXiv:0808.1089v1](https://arxiv.org/abs/0808.1089v1) [hep-ex] (2008).
  - [21] S. Moch and P. Uwer, *Nucl. Phys. Proc. Suppl.* **183**, 75 (2008) [[arXiv:0807.2794](https://arxiv.org/abs/0807.2794) [hep-ph]]; N. Kidonakis and R. Vogt, *Phys. Rev. D* **78**, 074005 (2008) [[arXiv:0805.3844](https://arxiv.org/abs/0805.3844) [hep-ph]].
  - [22] N. Kidonakis, *Phys. Rev. D* **74**, 114012 (2006) [[arXiv:hep-ph/0609287](https://arxiv.org/abs/hep-ph/0609287)].
  - [23] M.L. Mangano, M. Moretti, F. Piccinini, R. Pittau, A. Polosa, *JHEP* 0307:001; [hep-ph/0206293](https://arxiv.org/abs/hep-ph/0206293) (2003).
  - [24] T. Sjöstrand, L. Lonnblad and S. Mrenna, [arXiv:hep-ph/0108264](https://arxiv.org/abs/hep-ph/0108264) (2001); T. Sjöstrand, P. Eden, C. Friberg, L. Lonnblad, G. Miu, S. Mrenna and E. Norrbin, *Comput. Phys. Commun.* **135**, 238 (2001). [[arXiv:hep-ph/0010017](https://arxiv.org/abs/hep-ph/0010017)].
  - [25] CDF Collaboration, "Combined Upper Limit on Standard Model Higgs Boson Production for Summer 2008", CDF note 9502 (2008).
  - [26] N. Metropolis, A.W. Rosenbluth, M.N. Rosenbluth, A.H. Teller, and E. Teller. "Equations of State Calculations by Fast Computing Machines". *Journal of Chemical Physics*, 21(6):1087-1092, (1953). W.K. Hastings. "Monte Carlo Sampling Methods Using Markov Chains and Their Applications", *Biometrika*, 57(1):97-109, (1970).
  - [27] The ALEPH, DELPHI, L3 and OPAL Collaborations, and the LEP Higgs Working Group, *Phys. Lett. B* **565**, 61 (2003).
  - [28] The CDF and D0 Collaborations, and the Tevatron New Phenomena and Higgs Working Group, "Combined CDF and D0 Upper Limits on Standard Model Higgs-Boson Production with up to 4.2 fb<sup>-1</sup> of Data", [arXiv:0903.4001v1](https://arxiv.org/abs/0903.4001v1) [hep-ex], FERMILAB-PUB-09-060-E, CDF Note 9713, D0 Note 5889 (2009).

TABLE I: Analyzed integrated luminosities and references for the four main CDF SM Higgs search channels combined in this note

Channel	$\int \mathcal{L} dt$ (fb $^{-1}$ )	Reference
$WH \rightarrow \ell \nu b \bar{b}$ (triggered leptons+isotr)	4.3	[2]
$ZH \rightarrow \nu \bar{\nu} b \bar{b}$	3.6	[3]
$ZH \rightarrow \ell^+ \ell^- b \bar{b}$	4.1	[4]
$H \rightarrow \tau^+ \tau^-$	2.0	[5]
$WH + ZH \rightarrow jj b \bar{b}$	2.0	[6]
$H \rightarrow W^+ W^- \rightarrow \ell^+ \nu_{\ell'} \ell'^- \bar{\nu}_{\ell'}$	4.8	[7]

TABLE II: The (N)NLO production cross sections and decay branching fractions for the SM Higgs boson assumed for the combination

$m_H$ (GeV/ $c^2$ )	$\sigma_{gg \rightarrow H}$ (fb)	$\sigma_{WH}$ (fb)	$\sigma_{ZH}$ (fb)	$\sigma_{VBF}$ (fb)	$B(H \rightarrow b\bar{b})$ (%)	$B(H \rightarrow \tau^+ \tau^-)$ (%)	$B(H \rightarrow W^+ W^-)$ (%)
100	1861	286.1	166.7	99.5	81.21	7.924	1.009
105	1618	244.6	144.0	93.3	79.57	7.838	2.216
110	1413	209.2	124.3	87.1	77.02	7.656	4.411
115	1240	178.8	107.4	79.07	73.22	7.340	7.974
120	1093	152.9	92.7	71.65	67.89	6.861	13.20
125	967	132.4	81.1	67.37	60.97	6.210	20.18
130	858	114.7	70.9	62.5	52.71	5.408	28.69
135	764	99.3	62.0	57.65	43.62	4.507	38.28
140	682	86.0	54.2	52.59	34.36	3.574	48.33
145	611	75.3	48.0	49.15	25.56	2.676	58.33
150	548	66.0	42.5	45.67	17.57	1.851	68.17
155	492	57.8	37.6	42.19	10.49	1.112	78.23
160	439	50.7	33.3	38.59	4.00	0.426	90.11
165	389	44.4	29.5	36.09	1.265	0.136	96.10
170	349	38.9	26.1	33.58	0.846	0.091	96.53
175	314	34.6	23.3	31.11	0.663	0.072	95.94
180	283	30.7	20.8	28.57	0.541	0.059	93.45
190	231	24.3	16.6	24.88	0.342	0.038	77.61
200	192	19.3	13.5	21.19	0.260	0.029	73.47

TABLE III: Systematic uncertainties for the  $WH \rightarrow \ell\nu b\bar{b}$  analysis, for the SECVTX+JP channel, the SECVTX+ROMA channel, and the double-SECVTX tag channel. Systematic uncertainties are listed by name, see the original references for a detailed explanation of their meaning and on how they are derived. Systematic uncertainties for the  $WH$  signal shown in this table are obtained for  $m_H = 115 \text{ GeV}/c^2$ . Uncertainties are relative, in percent and are symmetric unless otherwise indicated.

SECVTX+JP  $WH \rightarrow \ell\nu b\bar{b}$   
analysis.

Contribution	W+HF	Mistags	Top	Diboson	Non-W	WH
Luminosity ( $\sigma_{\text{inel}}(p\bar{p})$ )	0	0	3.8	3.8	0	3.8
Luminosity Monitor	0	0	4.4	4.4	0	4.4
Lepton ID	0	0	2	2	0	2
Jet Energy Scale	0	0	0	0	0	2.8
Mistag Rate	0	36.0	0	0	0	0
B-Tag Efficiency	0	0	8.1	8.1	0	8.1
$t\bar{t}$ Cross Section	0	0	10	0	0	0
Diboson Rate	0	0	0	11.5	0	0
Signal Cross Section	0	0	0	0	0	5
HF Fraction in W+jets	45.0	0	0	0	0	0
ISR+FSR+PDF	0	0	0	0	0	4.9
QCD Rate	0	0	0	0	40	0

SECVTX+ROMA  $WH \rightarrow \ell\nu b\bar{b}$   
analysis.

Contribution	W+HF	Mistags	Top	Diboson	Non-W	WH
Luminosity ( $\sigma_{\text{inel}}(p\bar{p})$ )	0	0	3.8	3.8	0	3.8
Luminosity Monitor	0	0	4.4	4.4	0	4.4
Lepton ID	0	0	2	2	0	2
Jet Energy Scale	0	0	0	0	0	2.2
Mistag Rate	0	36.0	0	0	0	0
B-Tag Efficiency	0	0	13.6	13.6	0	13.6
$t\bar{t}$ Cross Section	0	0	10	0	0	0
Diboson Rate	0	0	0	11.5	0	0
Signal Cross Section	0	0	0	0	0	5
HF Fraction in W+jets	45.0	0	0	0	0	0
ISR+FSR+PDF	0	0	0	0	0	7.7
QCD Rate	0	0	0	0	40	0

Double-SECVTX Tagged  $WH \rightarrow \ell\nu b\bar{b}$   
analysis.

Contribution	W+HF	Mistags	Top	Diboson	Non-W	WH
Luminosity ( $\sigma_{\text{inel}}(p\bar{p})$ )	0	0	3.8	3.8	0	3.8
Luminosity Monitor	0	0	4.4	4.4	0	4.4
Lepton ID	0	0	2	2	0	2
Jet Energy Scale	0	0	0	0	0	2
Mistag Rate	0	35.0	0	0	0	0
B-Tag Efficiency	0	0	8.6	8.6	0	8.6
$t\bar{t}$ Cross Section	0	0	10	0	0	0
Diboson Rate	0	0	0	11.5	0	0
Signal Cross Section	0	0	0	0	0	5
HF Fraction in W+jets	45.0	0	0	0	0	0
ISR+FSR+PDF	0	0	0	0	0	4.9
QCD Rate	0	0	0	0	40	0

TABLE IV: Systematic uncertainties for the  $WH \rightarrow \ell\nu b\bar{b}$  analysis, for the single-SECVTX tag channel. Systematic uncertainties are listed by name, see the original references for a detailed explanation of their meaning and on how they are derived. Systematic uncertainties for the  $WH$  signal shown in this table are obtained for  $m_H = 115 \text{ GeV}/c^2$ . Uncertainties are relative, in percent and are symmetric unless otherwise indicated.

Single-SECVTX tag  $WH \rightarrow \ell\nu b\bar{b}$   
analysis.

Contribution	W+HF	Mistags	Top	Diboson	Non-W	WH
Luminosity ( $\sigma_{\text{inel}}(p\bar{p})$ )	0	0	3.8	3.8	0	3.8
Luminosity Monitor	0	0	4.4	4.4	0	4.4
Lepton ID	0	0	2	2	0	2
Jet Energy Scale	0	0	0	0	0	2.3
Mistag Rate	0	35.0	0	0	0	0
B-Tag Efficiency	0	0	4.3	4.3	0	4.3
$t\bar{t}$ Cross Section	0	0	10	0	0	0
Diboson Rate	0	0	0	11.5	0	0
Signal Cross Section	0	0	0	0	0	5
HF Fraction in W+jets	42.0	0	0	0	0	0
ISR+FSR+PDF	0	0	0	0	0	3.0
QCD Rate	0	0	0	0	40	0

TABLE V: Observed and expected limits for the six total  $WH \rightarrow \ell\nu b\bar{b}$  channels: (double tag + SECVTX+JP + SECVTX+ROMA, + single SECVTX) $\times$ (tight leptons+ forward electrons + isotrk). The observed and median expected limits in the background-only hypothesis are listed. Also listed are the limits from [2]. The limits are all given in units of  $R = \sigma/\sigma_{SM}$ , assuming SM branching fractions.

$m_H$ ( $\text{GeV}/c^2$ )	Observed limit/SM	median expected	CDF 9868 observed	CDF 9868 expected
100	4.20	2.97	3.98	2.78
105	4.60	3.38	4.47	3.12
110	5.02	3.79	5.01	3.48
115	5.18	4.28	5.26	3.98
120	4.65	5.06	4.88	4.62
125	6.66	6.54	7.01	5.99
130	7.08	7.75	7.53	7.36
135	11.24	10.9	11.8	10.1
140	14.69	15.1	15.7	14.1
145	23.78	22.9	25.0	21.8
150	35.59	36.5	37.6	33.7

TABLE VI: Systematic uncertainties for the  $WH, ZH \rightarrow \cancel{E}_T b\bar{b}$  SECVTX+SECVTX, SECVTX+JP, single-SECVTX channels. Systematic uncertainties are listed by name, see [3] for a detailed explanation of their meaning and on how they are derived. Systematic uncertainties for  $ZH$  and  $WH$  shown in this table are obtained for  $m_H = 120 \text{ GeV}/c^2$ . Uncertainties are relative, in percent and are symmetric unless otherwise indicated.

$WH, ZH \rightarrow \cancel{E}_T b\bar{b}$ SECVTX+SECVTX channel								
	ZH	WH	Multijet	Top Pair	S. Top	Di-boson	W + h.f.	Z + h.f.
<i>Correlated uncertainties</i>								
Luminosity	3.8	3.8		3.8	3.8	3.8	3.8	3.8
Lumi Monitor	4.4	4.4		4.4	4.4	4.4	4.4	4.4
Tagging SF	8.6	8.6		8.6	8.6	8.6	8.6	8.6
Trigger Eff. (shape)	1.0	1.2	1.1	0.7	1.1	1.6	1.7	1.3
Lepton Veto	2.0	2.0		2.0	2.0	2.0	2.0	2.0
PDF Acceptance	2.0	2.0		2.0	2.0	2.0	2.0	2.0
JES (shape)	+3.0 -3.0	+3.5 -4.7	-4.0 +3.8	+1.1 -1.1	+2.4 -4.7	+8.2 -6.1	+7.3 -11.8	+6.5 -8.3
ISR		+4.4						
FSR		+3.7						
		+1.8						
		+4.4						
<i>Uncorrelated uncertainties</i>								
Cross-Section	5	5		10	10	11.5	40	40
Multijet Norm. (shape)			17					

$WH, ZH \rightarrow \cancel{E}_T b\bar{b}$ SECVTX+JP channel								
	ZH	WH	Multijet	Top Pair	S. Top	Di-boson	W + h.f.	Z + h.f.
<i>Correlated uncertainties</i>								
Luminosity	3.8	3.8		3.8	3.8	3.8	3.8	3.8
Lumi Monitor	4.4	4.4		4.4	4.4	4.4	4.4	4.4
Tagging SF	9.1	9.1		9.1	9.1	9.1	9.1	9.1
Trigger Eff. (shape)	1.2	1.3	1.1	0.7	1.2	1.2	1.8	1.3
Lepton Veto	2.0	2.0		2.0	2.0	2.0	2.0	2.0
PDF Acceptance	2.0	2.0		2.0	2.0	2.0	2.0	2.0
JES (shape)	+3.7 -3.7	+4.0 -4.0	-5.4 +5.2	+1.1 -0.7	+4.2 -4.2	+7.0 -7.0	+1.3 -7.6	+6.2 -7.1
ISR		+1.4						
FSR		-2.9						
		+5.3						
		+2.5						
<i>Uncorrelated uncertainties</i>								
Cross-Section	5.0	5.0		10	10	11.5	40	40
Multijet Norm. (shape)			11					

$WH, ZH \rightarrow \cancel{E}_T b\bar{b}$ Single-SECVTX channel								
	ZH	WH	Multijet	Top Pair	S. Top	Di-boson	W + h.f.	Z + h.f.
<i>Correlated uncertainties</i>								
Luminosity	3.8	3.8		3.8	3.8	3.8	3.8	3.8
Lumi Monitor	4.4	4.4		4.4	4.4	4.4	4.4	4.4
Tagging SF	4.3	4.3		4.3	4.3	4.3	4.3	4.3
Trigger Eff. (shape)	0.9	1.1	1.1	0.7	1.1	1.3	2.0	1.4
Lepton Veto	2.0	2.0		2.0	2.0	2.0	2.0	2.0
PDF Acceptance	2.0	2.0		2.0	2.0	2.0	2.0	2.0
JES (shape)	+3.8 -3.8	+3.8 -3.8	-5.2 +5.6	+0.7 -0.8	+4.6 -4.6	+7.0 -5.6	+12.4 -12.7	+8.3 -8.1
ISR		-1.0						
FSR		-1.5						
		+2.0						
		-0.1						
<i>Uncorrelated uncertainties</i>								
Cross-Section	5.0	5.0		10	10	11.5	40	40
Multijet Norm. (shape)			3.9					



Double SECVTX Tag High S/B (TDT High)  $ZH \rightarrow \ell\ell b\bar{b}$  Analysis

Contribution	Fakes	Top	$WZ$	$ZZ$	$Z + b\bar{b}$	$Z + c\bar{c}$	$Z + \text{mistag}$	$ZH$
Luminosity ( $\sigma_{\text{inel}}(p\bar{p})$ )	0	3.8	3.8	3.8	3.8	3.8	0	3.8
Luminosity Monitor	0	4.4	4.4	4.4	4.4	4.4	0	4.4
Lepton ID	0	1	1	1	1	1	0	1
Lepton Energy Scale	0	1.5	1.5	1.5	1.5	1.5	0	1.5
$ZH$ Cross Section	0	0	0	0	0	0	0	5
Fake Leptons	50	0	0	0	0	0	0	0
Jet Energy Scale (shape dep.)	0	+1.6 -1.1	+0.0 -0.0	+1.8 -2.7	+5.9 -6.8	+6.0 -5.9	0	+2.0 +0.01
Mistag Rate (shape dep.)	0	0	0	0	0	0	+30.7 -26.6	0
B-Tag Efficiency	0	8	8	8	8	8	0	8
$t\bar{t}$ Cross Section	0	20	0	0	0	0	0	0
Diboson Cross Section	0	0	11.5	11.5	0	0	0	0
$\sigma(p\bar{p} \rightarrow Z + HF)$	0	0	0	0	40	40	0	0
ISR (shape dep.)	0	0	0	0	0	0	0	-2.0 +1.2
FSR (shape dep.)	0	0	0	0	0	0	0	-0.01 +0.01

Double SECVTX Tag Low S/B (TDT Low)  $ZH \rightarrow \ell\ell b\bar{b}$  Analysis

Contribution	Fakes	Top	$WZ$	$ZZ$	$Z + b\bar{b}$	$Z + c\bar{c}$	$Z + \text{mistag}$	$ZH$
Luminosity ( $\sigma_{\text{inel}}(p\bar{p})$ )	0	3.8	3.8	3.8	3.8	3.8	0	3.8
Luminosity Monitor	0	4.4	4.4	4.4	4.4	4.4	0	4.4
Lepton ID	0	1	1	1	1	1	0	1
Lepton Energy Scale	0	1.5	1.5	1.5	1.5	1.5	0	1.5
$ZH$ Cross Section	0	0	0	0	0	0	0	5
Fake Leptons	50	0	0	0	0	0	0	0
Jet Energy Scale (shape dep.)	0	$^{+0.01}_{-0.01}$	$^{+0.0}_{-0.0}$	$^{+0.0}_{-3.2}$	$^{+5.8}_{-6.3}$	$^{+7.1}_{-5.8}$	0	$^{+2.3}_{+0.0}$
Mistag Rate (shape dep.)	0	0	0	0	0	0	$^{+31.5}_{-27.2}$	0
B-Tag Efficiency	0	8	8	8	8	8	0	8
$t\bar{t}$ Cross Section	0	20	0	0	0	0	0	0
Diboson Cross Section	0	0	11.5	11.5	0	0	0	0
$\sigma(p\bar{p} \rightarrow Z + HF)$	0	0	0	0	40	40	0	0
ISR (shape dep.)	0	0	0	0	0	0	0	$^{-0.01}_{+0.0}$
FSR (shape dep.)	0	0	0	0	0	0	0	$^{-4.3}_{-0.01}$

SECVTX + JP Tag High S/B (LDT High)  $ZH \rightarrow \ell\ell b\bar{b}$  Analysis

Contribution	Fakes	Top	$WZ$	$ZZ$	$Z + b\bar{b}$	$Z + c\bar{c}$	$Z + \text{mistag}$	$ZH$
Luminosity ( $\sigma_{\text{inel}}(p\bar{p})$ )	0	3.8	3.8	3.8	3.8	3.8	0	3.8
Luminosity Monitor	0	4.4	4.4	4.4	4.4	4.4	0	4.4
Lepton ID	0	1	1	1	1	1	0	1
Lepton Energy Scale	0	1.5	1.5	1.5	1.5	1.5	0	1.5
$ZH$ Cross Section	0	0	0	0	0	0	0	5
Fake Leptons	50	0	0	0	0	0	0	0
Jet Energy Scale (shape dep.)	0	$^{+1.3}_{-0.01}$	$^{+3.1}_{-4.3}$	$^{+3.1}_{-3.0}$	$^{+7.5}_{-7.3}$	$^{+6.2}_{-6.0}$	0	$^{+1.9}_{+0.0}$
Mistag Rate (shape dep.)	0	0	0	0	0	0	$^{+33.6}_{-26.4}$	0
B-Tag Efficiency	0	11	11	11	11	11	0	11
$t\bar{t}$ Cross Section	0	20	0	0	0	0	0	0
Diboson Cross Section	0	0	11.5	11.5	0	0	0	0
$\sigma(p\bar{p} \rightarrow Z + HF)$	0	0	0	0	40	40	0	0
ISR (shape dep.)	0	0	0	0	0	0	0	$^{+3.0}_{+0.0}$
FSR (shape dep.)	0	0	0	0	0	0	0	$^{+1.4}_{-0.0}$

SECVTX + JP Tag Low S/B (LDT Low)  $ZH \rightarrow \ell\ell b\bar{b}$  Analysis

Contribution	Fakes	Top	$WZ$	$ZZ$	$Z + b\bar{b}$	$Z + c\bar{c}$	$Z + \text{mistag}$	$ZH$
Luminosity ( $\sigma_{\text{inel}}(p\bar{p})$ )	0	3.8	3.8	3.8	3.8	3.8	0	3.8
Luminosity Monitor	0	4.4	4.4	4.4	4.4	4.4	0	4.4
Lepton ID	0	1	1	1	1	1	0	1
Lepton Energy Scale	0	1.5	1.5	1.5	1.5	1.5	0	1.5
$ZH$ Cross Section	0	0	0	0	0	0	0	5
Fake Leptons	50	0	0	0	0	0	0	0
Jet Energy Scale (shape dep.)	0	$^{+1.7}_{-0.0}$	$^{-0.0}_{-5.9}$	$^{+2.9}_{-0.01}$	$^{+8.2}_{-8.8}$	$^{+8.1}_{-8.8}$	0	$^{+2.7}_{-0.0}$
Mistag Rate (shape dep.)	0	0	0	0	0	0	$^{+34.5}_{-27.8}$	0
B-Tag Efficiency	0	11	11	11	11	11	0	11
$t\bar{t}$ Cross Section	0	20	0	0	0	0	0	0
Diboson Cross Section	0	0	11.5	11.5	0	0	0	0
$\sigma(p\bar{p} \rightarrow Z + HF)$	0	0	0	0	40	40	0	0
ISR (shape dep.)	0	0	0	0	0	0	0	$^{+4.1}_{+7.8}$
FSR (shape dep.)	0	0	0	0	0	0	0	$^{+23.5}_{+9.9}$

TABLE VIII: Observed and expected limits for the  $ZH \rightarrow \ell^+ \ell^- b \bar{b}$  channels, with the single-tag and double-tag analyses combined. The observed and median expected limits are listed. Also listed are the limits from [4]. The limits are all given in units of  $R = \sigma/\sigma_{SM}$ , assuming SM branching fractions.

$m_H$ (GeV/ $c^2$ )	Observed limit/SM	median expected	CDF 9889 observed	CDF 9889 expected
100	4.67	6.76	4.53	6.7
105	5.07	6.47	4.6	6.38
110	5.56	6.46	5.25	6.34
115	6.15	7.10	5.91	6.8
120	7.91	8.56	7.89	8.49
125	9.05	10.0	8.14	10.21
130	11.00	13.30	10.3	12.79
135			14.41	18.74
140			19.27	28.49
145			24.22	45.34
150			42.93	73.72

TABLE IX: Systematic uncertainties on the contributions for the  $H \rightarrow \tau^+ \tau^-$  channel. Systematic uncertainties are listed by name, see the original references for a detailed explanation of their meaning and on how they are derived. Uncertainties with provided shape systematics are labeled with “s”. Systematic uncertainties for  $H$  shown in this table are obtained for  $m_H = 115$  GeV/ $c^2$ . Uncertainties are relative, in percent and are symmetric unless otherwise indicated. The systematic uncertainty called “Normalization” includes effects of the inelastic  $p\bar{p}$  cross section, the luminosity monitor acceptance, and the lepton trigger acceptance. It is considered to be entirely correlated with the luminosity uncertainty.

Contribution	$Z/\gamma^* \rightarrow \tau\tau$	$Z/\gamma^* \rightarrow \ell\ell$	$t\bar{t}$	diboson	jet $\rightarrow \tau$	W+jet	WH	ZH	VBF	$gg \rightarrow H$
Luminosity	3.8	3.8	3.8	3.8	-	-	3.8	3.8	3.8	3.8
Luminosity Monitor	4.4	4.4	4.4	4.4	-	-	4.4	4.4	4.4	4.4
$e, \mu$ Trigger	1	1	1	1	-	-	1	1	1	1
$\tau$ Trigger	3	3	3	3	-	-	3	3	3	3
$e, \mu, \tau$ ID	3	3	3	3	-	-	3	3	3	3
PDF Uncertainty	1	1	1	1	-	-	1	1	1	1
ISR/FSR	-	-	-	-	-	-	2/0	1/1	3/1	12/1
JES (shape)	16	13	2	10	-	-	3	3	4	14
Cross Section or Norm.	2	2	10	11.5	-	15	5	5	10	10
MC model	20	10	-	-	-	-	-	-	-	-

TABLE X: Observed and expected limits for the  $H \rightarrow \tau^+ \tau^-$  channel. The observed and median expected limits are listed. Also listed are the limits from [5]. The limits are all given in units of  $R = \sigma/\sigma_{SM}$ , assuming SM branching fractions.

$m_H$ (GeV/ $c^2$ )	Observed limit/SM	median expected	CDF 9179 observed	CDF 9179 expected
110	30.29	25.9	32.5	25.8
115	31.12	24.4	30.5	24.8
120	29.66	24.6	30.0	24.2
125	28.96	25.5		
130	37.44	33.4	39.5	32.3
135	44.06	36.6		
140	62.77	51.6	67.5	52.8
145	91.95	73.3		
150	149.23	120	159.0	111.7

TABLE XI: Systematic uncertainties summary for CDF’s  $WH + ZH \rightarrow jjb\bar{b}$  channel [6]. Systematic uncertainties are listed by name, see the original references for a detailed explanation of their meaning and on how they are derived. Uncertainties with provided shape systematics are labeled with “s”. Systematic uncertainties for  $H$  shown in this table are obtained for  $m_H = 115$  GeV/ $c^2$ . Uncertainties are relative, in percent and are symmetric unless otherwise indicated. The cross section uncertainties are uncorrelated with each other (except for single top and  $t\bar{t}$ , which are treated as correlated). The QCD uncertainty is also uncorrelated with other channels’ QCD rate uncertainties.

CDF:  $WH + ZH \rightarrow jjb\bar{b}$  Analysis

	QCD	$t\bar{t}$	$Wb\bar{b}$	$WZ$	Single Top	$Z$ +jets	$WH$	$ZH$
Interpolation	0s	–	–	–	–	–	–	–
MC Modeling	0s	–	–	–	–	–	18s	16s
Cross Section	10	10	30	6	10	30	5	5

TABLE XII: Observed and expected limits for the  $WH + ZH \rightarrow jjb\bar{b}$  channel. The observed and median expected limits are listed. Also listed are the limits from [6]. The limits are all given in units of  $R = \sigma/\sigma_{SM}$ , assuming SM branching fractions.

$m_H$ (GeV/ $c^2$ )	Observed limit/SM	median expected	CDF 9366 observed	CDF 9366 expected
100	28.1	26.8	29.7	28.7
105	38.2	33.3	37.6	33.7
110	34.3	36.2	38.7	36.6
115	36.3	40.0	37.5	36.8
120	36.0	44.9	38.2	39.6
125	40.5	57.2	43.4	46.8
130	43.7	68.3	48.0	53.6
135	57.7	88.9	73.6	80.2
140	74.6	126	107	115
145	116	187	163	176
150	177	305	261	287

TABLE XIII: Systematic uncertainties on the contributions for the  $H \rightarrow W^+W^- \rightarrow \ell^\pm \ell'^\mp$  channels with zero, one, and two or more associated jets. These channels are sensitive to gluon fusion production (all channels) and  $WH, ZH$  and VBF production (channels with one or more associated jets). Systematic uncertainties are listed by name. See [7] for details of how the uncertainties are estimated. Systematic uncertainties for the signal shown in this table are obtained for  $m_H = 160 \text{ GeV}/c^2$ . Uncertainties are relative, in percent and are symmetric unless otherwise indicated. The uncertainties associated with the different background and signal processed are correlated within individual categories unless otherwise noted. In these special cases, the correlated uncertainties are shown in either italics or bold face text. Monte Carlo statistical uncertainties in each bin of each template are considered as independent systematic uncertainties. All uncertainty categories are treated as correlated between channels with the exception of the Missing Et Modeling uncertainty.

$H \rightarrow W^+W^- \rightarrow \ell^\pm \ell'^\mp$ channels with no associated jet											
Uncertainty Source	$WW$	$WZ$	$ZZ$	$t\bar{t}$	DY	$W\gamma$	$W+\text{jet(s)}$	$gg \rightarrow H$			
Cross Section	<i>6.0</i>	<i>6.0</i>	<i>6.0</i>	10.0	5.0				10.4		
Scale (leptons)									2.5		
Scale (jets)									4.6		
PDF Model (leptons)	1.9	2.7	2.7	2.1	4.1				1.5		
PDF Model (jets)									0.9		
Higher-order Diagrams	<i>5.0</i>	<i>10.0</i>	<i>10.0</i>	10.0			11.0				
Missing Et Modeling						21.0					
$W\gamma$ Scaling							12.0				
Jet Fake Rates (Low/High S/B)									21.5/27.7		
Jet Modeling	-1.0						-4.0				
MC Run Dependence	2.8										
Lepton ID Efficiencies	2.0	1.7	2.0	2.0	1.9				1.9		
Trigger Efficiencies	2.1	2.1	2.1	2.0	3.4				3.3		
Luminosity	3.8	3.8	3.8	3.8	3.8				3.8		
Luminosity Monitor	4.4	4.4	4.4	4.4	4.4				4.4		

$H \rightarrow W^+W^- \rightarrow \ell^\pm \ell'^\mp$ channels with one associated jet											
Uncertainty Source	$WW$	$WZ$	$ZZ$	$t\bar{t}$	DY	$W\gamma$	$W+\text{jet(s)}$	$gg \rightarrow H$	$WH$	$ZH$	VBF
Cross Section	<i>6.0</i>	<i>6.0</i>	<i>6.0</i>	10.0	5.0			24.7	<b>5.0</b>	<b>5.0</b>	10.0
Scale (leptons)								2.8			
Scale (jets)								-5.1			
PDF Model (leptons)	1.9	2.7	2.7	2.1	4.1			1.7	1.2	0.9	2.2
PDF Model (jets)								-1.9			
Higher-order Diagrams	<i>5.0</i>	<i>10.0</i>	<i>10.0</i>	10.0		11.0			<b>10.0</b>	<b>10.0</b>	<b>10.0</b>
Missing Et Modeling					30.0						
$W\gamma$ Scaling						12.0					
Jet Fake Rates (Low/High S/B)							22.2/31.5				
Jet Modeling	-1.0					15.0					
MC Run Dependence	1.0										
Lepton ID Efficiencies	2.0	2.0	2.2	1.8	2.0			1.9	1.9	1.9	1.9
Trigger Efficiencies	2.1	2.1	2.1	2.0	3.4			3.3	2.1	2.1	3.3
Luminosity	3.8	3.8	3.8	3.8	3.8			3.8	3.8	3.8	3.8
Luminosity Monitor	4.4	4.4	4.4	4.4	4.4			4.4	4.4	4.4	4.4

$H \rightarrow W^+W^- \rightarrow \ell^\pm \ell'^\mp$  channel with two or more associated jets

Uncertainty Source	$WW$	$WZ$	$ZZ$	$t\bar{t}$	DY	$W\gamma$	$W+\text{jet(s)}$	$gg \rightarrow H$	$WH$	$ZH$	VBF
Cross Section	<i>6.0</i>	<i>6.0</i>	<i>6.0</i>	10.0	5.0			67.9	<b>5.0</b>	<b>5.0</b>	10.0
Scale (leptons)								3.1			
Scale (jets)								-8.7			
PDF Model (leptons)	1.9	2.7	2.7	2.1	4.1			2.0	1.2	0.9	2.2
PDF Model (jets)								-2.8			
Higher-order Diagrams	<i>5.0</i>	<i>10.0</i>	<i>10.0</i>	10.0		11.0			<b>10.0</b>	<b>10.0</b>	<b>10.0</b>
Missing Et Modeling					32.0						
$W\gamma$ Scaling						12.0					
Jet Fake Rates							27.1				
Jet Modeling	20.0					18.5					
$b$ -tag veto				5.4							
MC Run Dependence	1.5										
Lepton ID Efficiencies	1.9	2.9	1.9	1.9	1.9			1.9	1.9	1.9	1.9
Trigger Efficiencies	2.1	2.1	2.1	2.0	3.4			3.3	2.1	2.1	3.3
Luminosity	3.8	3.8	3.8	3.8	3.8			3.8	3.8	3.8	3.8
Luminosity Monitor	4.4	4.4	4.4	4.4	4.4			4.4	4.4	4.4	4.4

TABLE XIV: Systematic uncertainties on the contributions for the  $H \rightarrow W^+W^- \rightarrow \ell^\pm \ell'^\mp$  low- $M_{\ell\ell}$  channel with zero or one associated jets. This channel is sensitive to only gluon fusion production. Systematic uncertainties are listed by name (see the original references for a detailed explanation of their meaning and on how they are derived). Systematic uncertainties for  $H$  shown in this table are obtained for  $m_H = 160 \text{ GeV}/c^2$ . Uncertainties are relative, in percent and are symmetric unless otherwise indicated. The uncertainties associated with the different background and signal processed are correlated within individual categories unless otherwise noted. In these special cases, the correlated uncertainties are shown in either italics or bold face text. Monte Carlo statistical uncertainties in each bin of each template are considered as independent systematic uncertainties. All uncertainty categories are treated as correlated between channels with the exception of the Missing Et Modeling uncertainty.

CDF:  $H \rightarrow W^+W^- \rightarrow \ell^\pm \ell'^\mp$  low  $M_{\ell\ell}$  channel with zero or one associated jets

Uncertainty Source	$WW$	$WZ$	$ZZ$	$t\bar{t}$	DY	$W\gamma$	$W+\text{jet(s)}$	$gg \rightarrow H$
Cross Section	<i>6.0</i>	<i>6.0</i>	<i>6.0</i>	10.0	5.0			14.3
Scale (leptons)								2.6
Scale (jets)								1.1
PDF Model (leptons)	1.9	2.7	2.7	2.1	4.1			1.7
PDF Model (jets)								0.3
Higher-order Diagrams	<i>5.5</i>	<i>11.0</i>	<i>11.0</i>	10.0				
Missing Et Modeling					22.0			
$W\gamma$ Scaling						12.0		
Jet Fake Rates							24.1	
Jet Modeling	-1.0							
MC Run Dependence	5.0							
Lepton ID Efficiencies	2.0	1.7	2.0	2.0	1.9			1.9
Trigger Efficiencies	2.1	2.1	2.1	2.0	3.4			3.3
Luminosity	3.8	3.8	3.8	3.8	3.8			3.8
Luminosity Monitor	4.4	4.4	4.4	4.4	4.4			4.4

core

TABLE XV: Systematic uncertainties on the contributions for the  $WH \rightarrow WWW \rightarrow \ell^\pm \ell'^\pm$  channel with one or more associated jets. This channel is sensitive to only  $WH$  and  $ZH$  production. Systematic uncertainties are listed by name (see the original references for a detailed explanation of their meaning and on how they are derived). Systematic uncertainties for  $H$  shown in this table are obtained for  $m_H = 160 \text{ GeV}/c^2$ . Uncertainties are relative, in percent and are symmetric unless otherwise indicated. The uncertainties associated with the different background and signal processes are correlated within individual categories unless otherwise noted. In these special cases, the correlated uncertainties are shown in either italics or bold face text. Monte Carlo statistical uncertainties in each bin of each template are considered as independent systematic uncertainties. All uncertainty categories are treated as correlated between channels with the exception of the Missing Et Modeling uncertainty.

$WH \rightarrow WWW \rightarrow \ell^\pm \ell'^\pm$  Analysis.

Uncertainty Source	$WW$	$WZ$	$ZZ$	$t\bar{t}$	DY	$W\gamma$	$W+\text{jet(s)}$	$WH$	$ZH$
Cross Section	<i>6.0</i>	<i>6.0</i>	<i>6.0</i>	10.0	5.0			<b>5.0</b>	<b>5.0</b>
Scale (leptons)									
Scale (jets)									
PDF Model (leptons)	1.9	2.7	2.7	2.1	4.1			1.2	0.9
PDF Model (jets)									
Higher-order Diagrams	<i>5.0</i>	<i>10.0</i>	<i>10.0</i>	10.0		11.0		<b>10.0</b>	<b>10.0</b>
Missing Et Modeling					17.0				
$W\gamma$ Scaling						12.0			
Jet Fake Rates							30.0		
Jet Modeling	3.0					<i>16.0</i>			
Charge Misassignment	16.5			16.5	16.5				
MC Run Dependence	1.0								
Lepton ID Efficiencies	2.0	2.0	2.0	2.0	2.0			2.0	2.0
Trigger Efficiencies	2.1	2.1	2.1	2.0	3.4			2.1	2.1
Luminosity	3.8	3.8	3.8	3.8	3.8			3.8	3.8
Luminosity Monitor	4.4	4.4	4.4	4.4	4.4			4.4	4.4

TABLE XVI: Observed and expected limits for the  $gg \rightarrow H \rightarrow W^+W^- \rightarrow \ell^+ \nu_\ell \ell'^- \bar{\nu}_{\ell'}$  channels, with the high- $s/b$  and low- $s/b$  analyses combined, for all three jet categories. The five opposite-sign channels and the one same-sign channel are combined. The observed and median expected limits are listed. Also listed are the limits from [7]. The limits are all given in units of  $R = \sigma/\sigma_{SM}$ , assuming SM branching fractions.

$m_H$ (GeV/ $c^2$ )	Observed limit/SM	median expected	CDF 9887 observed	CDF 9887 expected
100	130.13	87.6		
105	67.85	47.3		
110	39.13	27.4	38.76	24.72
115	17.35	13.1		
120	11.81	9.05	11.04	8.49
125	6.81	5.85		
130	5.42	4.67	5.04	4.28
135				
140			3.68	2.80
145			2.75	2.40
150			2.37	2.00
155	1.78	1.69	1.83	1.65
160	1.24	1.29	1.27	1.26
165	1.19	1.23	1.23	1.21
170	1.64	1.48	1.64	1.45
175	1.72	1.75	1.78	1.72
180	2.15	2.11	2.13	2.07
190	3.70	3.26	3.86	3.24
200	6.50	4.43	6.69	4.52

TABLE XVII: Observed and expected limits for all CDF SM Higgs boson search channels combined. The observed and median expected limits are listed, as well as  $\pm 1, 2\sigma$  variation on the expected limits from statistical fluctuations assuming only background processes contribute. The limits are all given in units of  $R = \sigma/\sigma_{SM}$ , assuming SM branching fractions.

$m_H$ (GeV/ $c^2$ )	Observed limit/SM	$-2\sigma$ expected	$-1\sigma$ expected	median expected	$+1\sigma$ expected	$+2\sigma$ expected
100	2.79	1.10	1.48	2.06	2.89	3.98
105	2.98	1.14	1.58	2.21	3.09	4.21
110	3.29	1.24	1.69	2.36	3.32	4.57
115	3.62	1.38	1.83	2.53	3.52	4.84
120	3.84	1.59	2.15	2.97	4.11	5.59
125	4.49	1.69	2.26	3.11	4.29	5.83
130	4.14	1.69	2.25	3.14	4.42	6.12
135	3.96	1.51	2.05	2.85	3.95	5.38
140	3.61	1.52	2.00	2.77	3.90	5.41
145	2.67	1.32	1.75	2.44	3.44	4.78
150	2.27	1.11	1.49	2.12	3.02	4.23
155	1.78	0.86	1.20	1.69	2.36	3.23
160	1.24	0.65	0.90	1.29	1.84	2.58
165	1.19	0.65	0.86	1.23	1.79	2.57
170	1.64	0.76	1.03	1.48	2.18	3.15
175	1.72	0.91	1.23	1.75	2.53	3.60
180	2.15	1.02	1.44	2.11	3.11	4.48
190	3.70	1.61	2.25	3.26	4.74	6.75
200	6.50	2.22	3.11	4.43	6.25	8.66

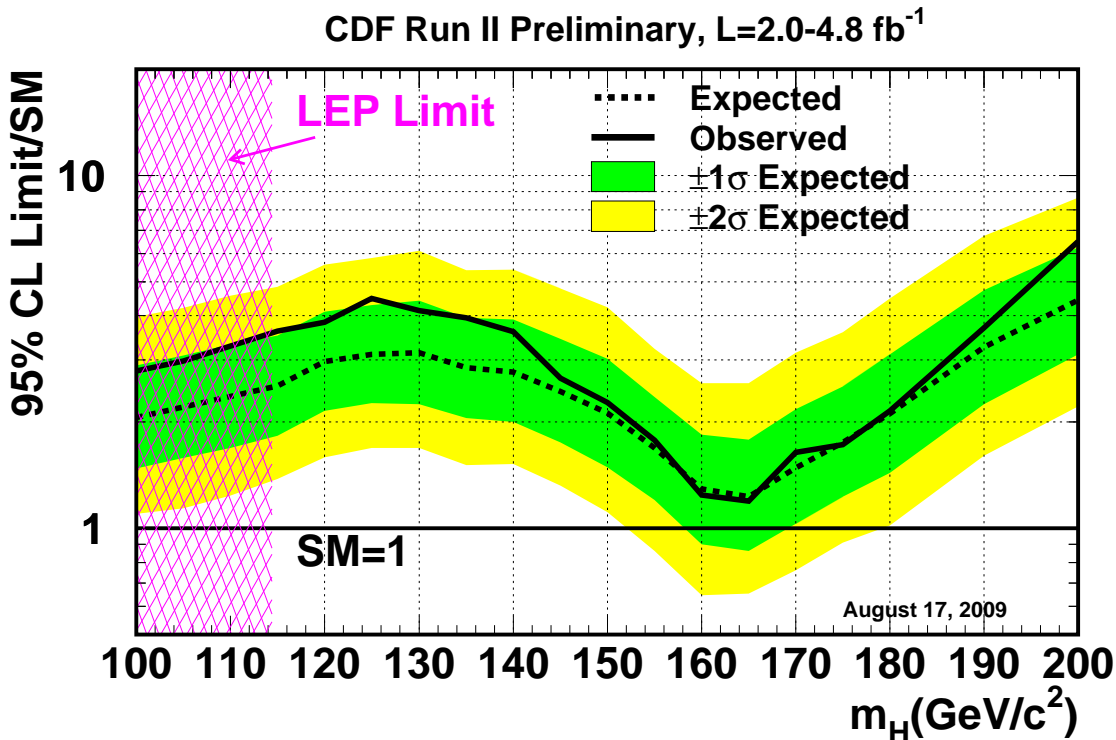


FIG. 1: The 95% CL upper limit on  $R = \sigma/\sigma_{\text{SM}}$ , shown as a function of  $m_H$ , for the combination of all of CDF's SM Higgs search channels. The  $\pm 1, 2\sigma$  bands on the expected limits are also shown, centered on the median expected limit.

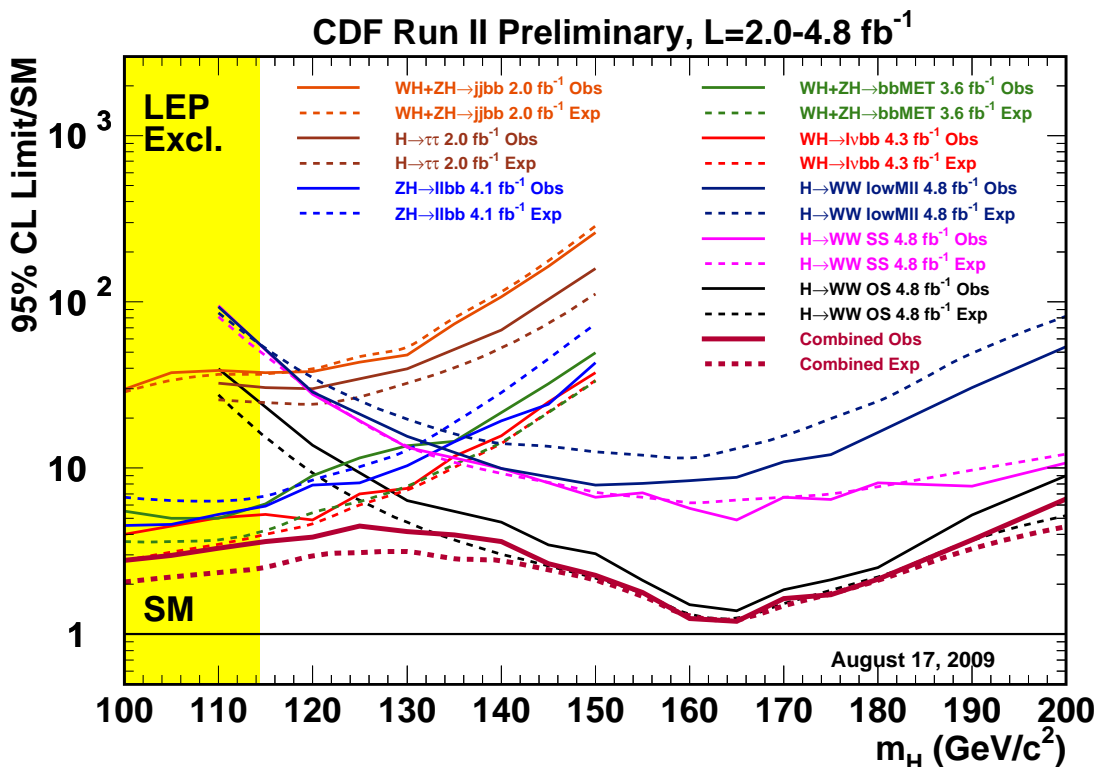


FIG. 2: The 95% CL upper limit on  $R = \sigma/\sigma_{\text{SM}}$ , shown as a function of  $m_H$ , shown separately for each analysis and for the combination. Dashed lines indicate the median expected limits, and the solid lines show the observed limits. The individual analysis limits are those approved by the individual analyses, and the combined limit is documented in this note. The LEP bound  $m_H > 114.4 \text{ GeV}/c^2$  is shown in yellow.

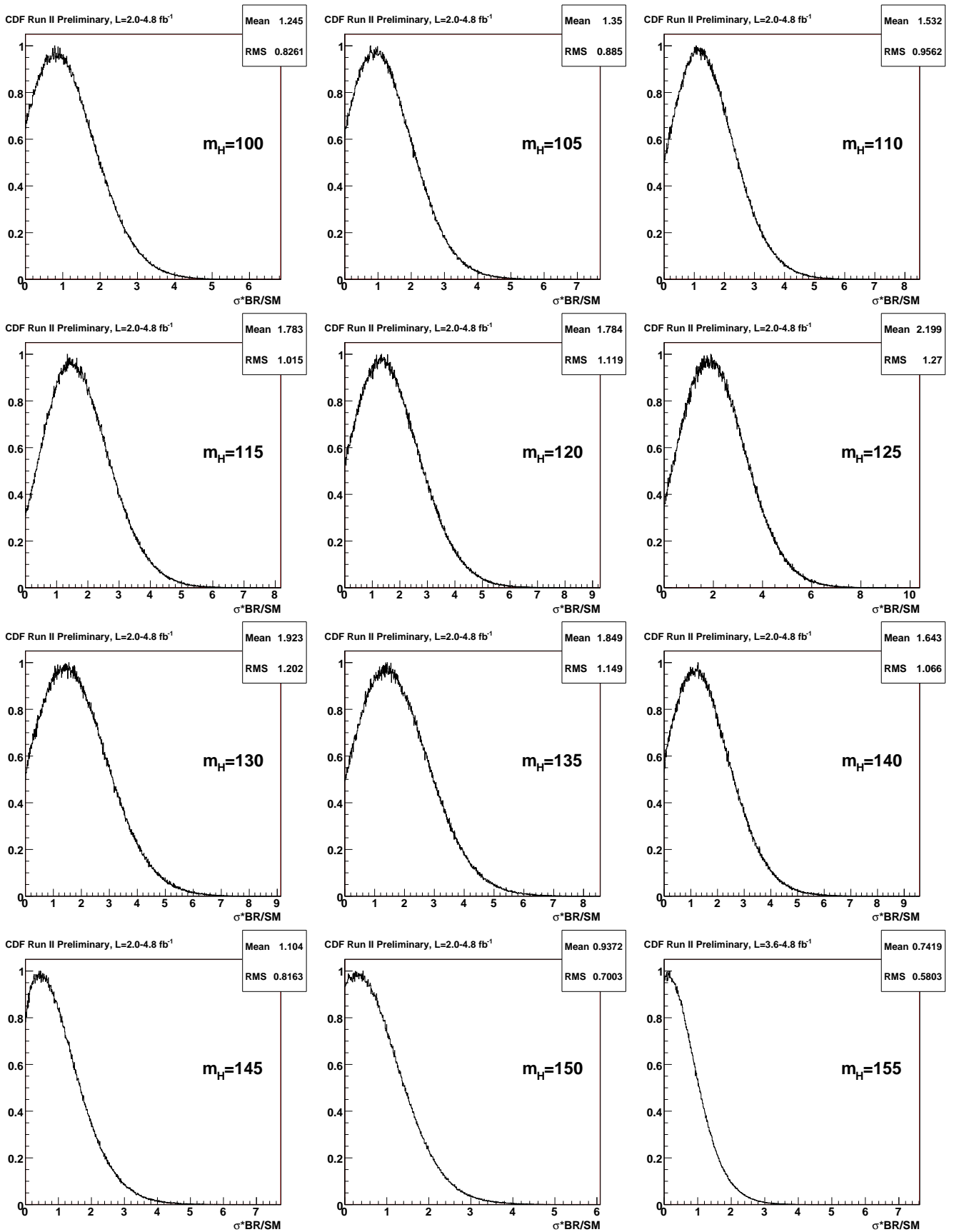


FIG. 3: The posterior densities and observed upper limits on  $R = \sigma/\sigma_{\text{SM}}$ , shown separately shown for Higgs boson masses of 100 through 155  $\text{GeV}/c^2$ .

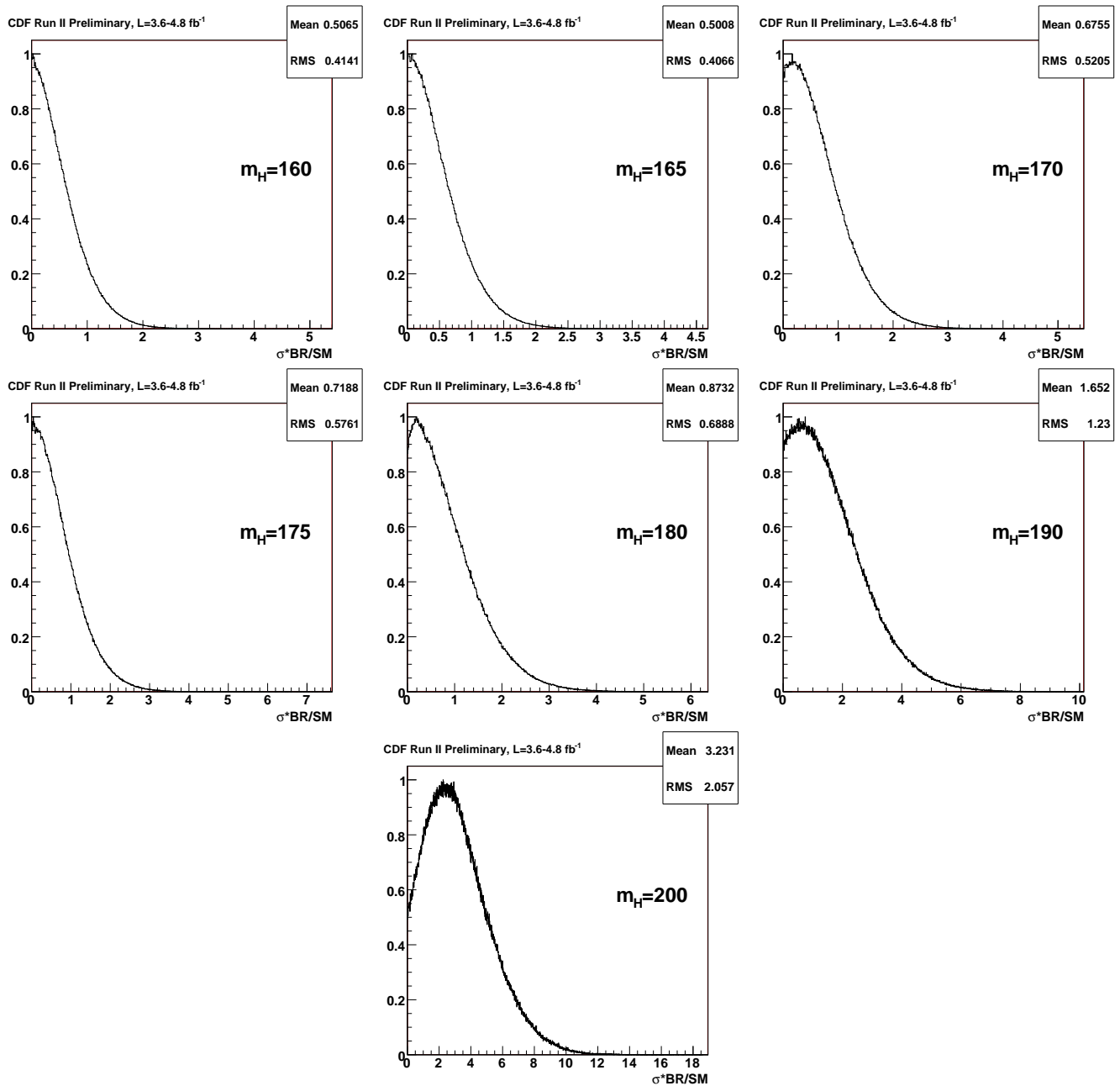


FIG. 4: The posterior densities and observed upper limits on  $R = \sigma/\sigma_{SM}$ , shown separately shown for Higgs boson masses of 160 through 200  $\text{GeV}/c^2$ .

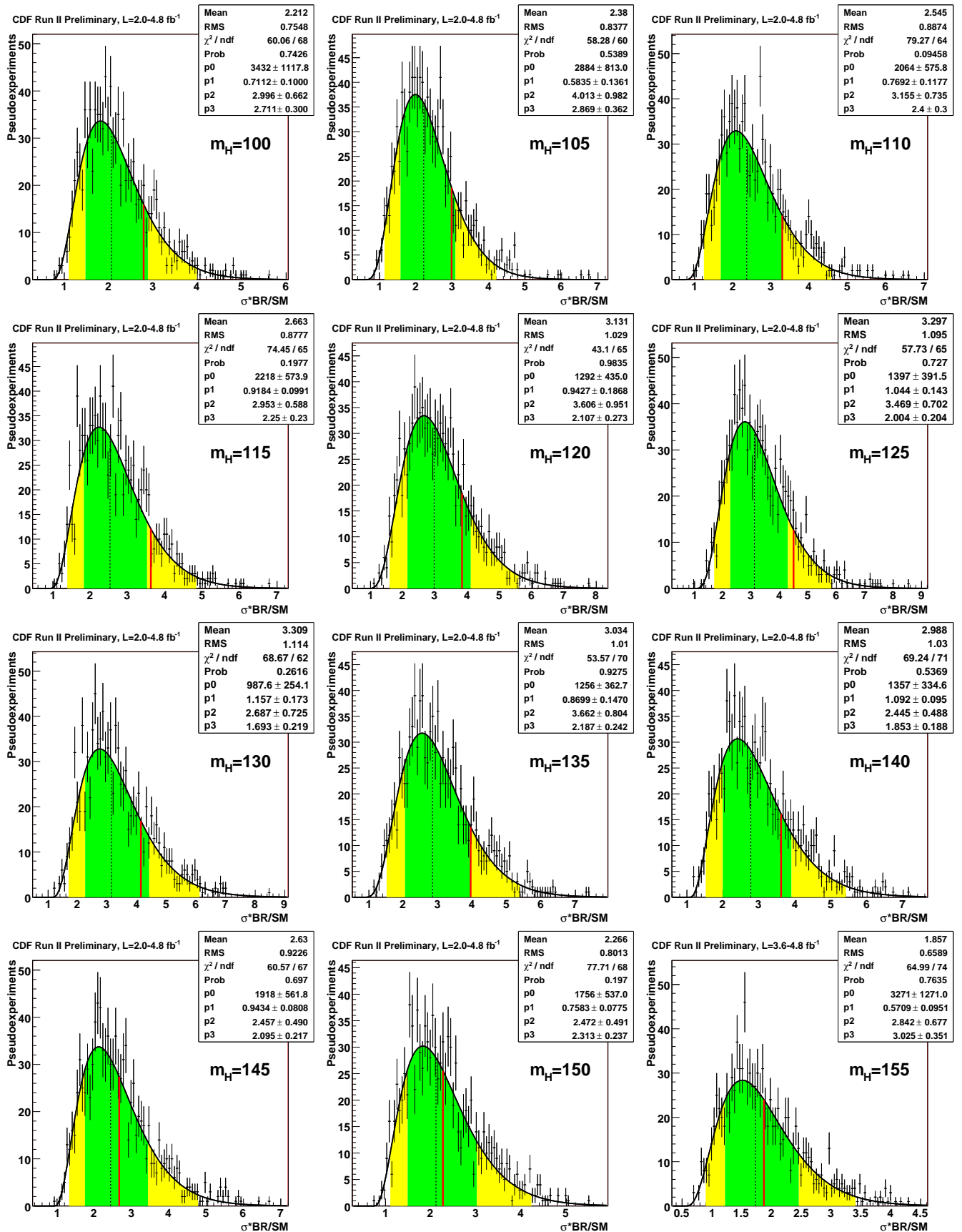


FIG. 5: The distributions of expected upper limits on  $R = \sigma/\sigma_{\text{SM}}$  assuming no signal is truly present in the data, separately shown for Higgs boson masses of 100 through 155  $\text{GeV}/c^2$ .

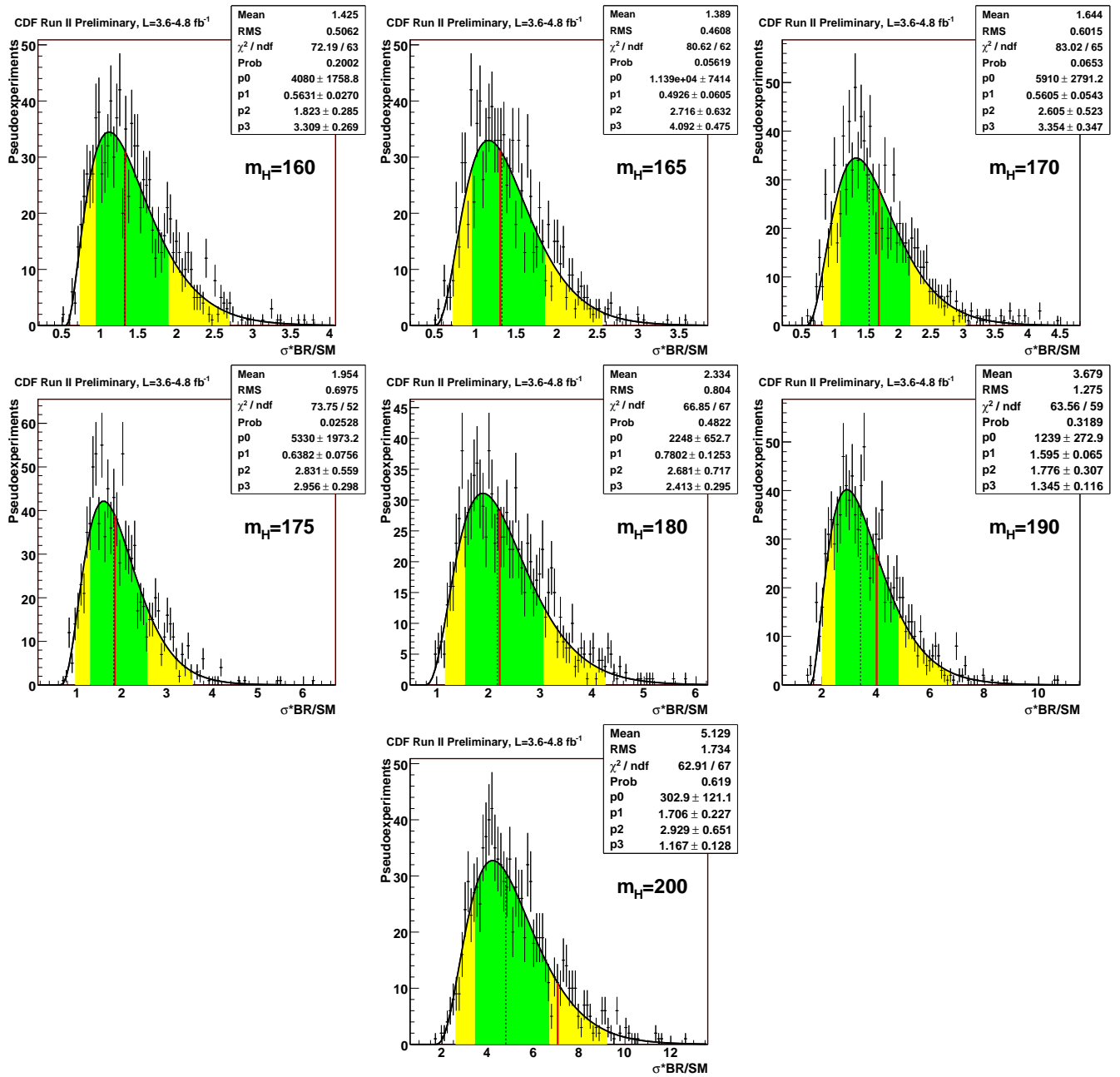


FIG. 6: The distributions of expected upper limits on  $R = \sigma/\sigma_{\text{SM}}$  assuming no signal is truly present in the data, separately shown for Higgs boson masses of 160 through 200  $\text{GeV}/c^2$ .

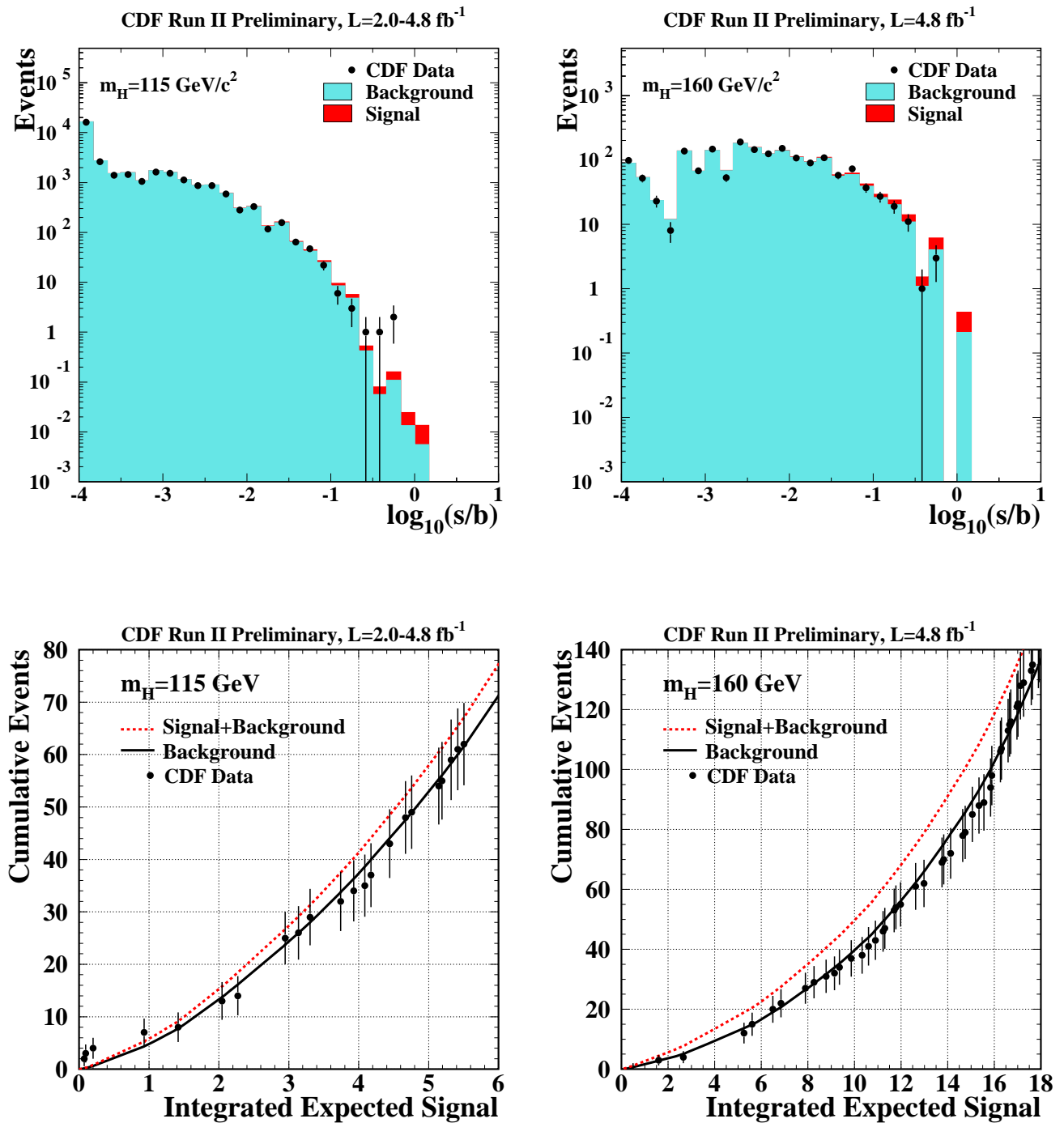


FIG. 7: Top plots: signal predictions, background predictions, and observed data, collected in bins sorted by  $s/b$ , for all channels added together. These are shown for  $m_H = 115$  and  $160 \text{ GeV}/c^2$ . Bottom plots: Integrated signal predictions, background predictions, and observed data, collected in bins sorted by  $s/b$ , for all channels added together. These are shown for  $m_H = 115$  and  $160 \text{ GeV}/c^2$ .

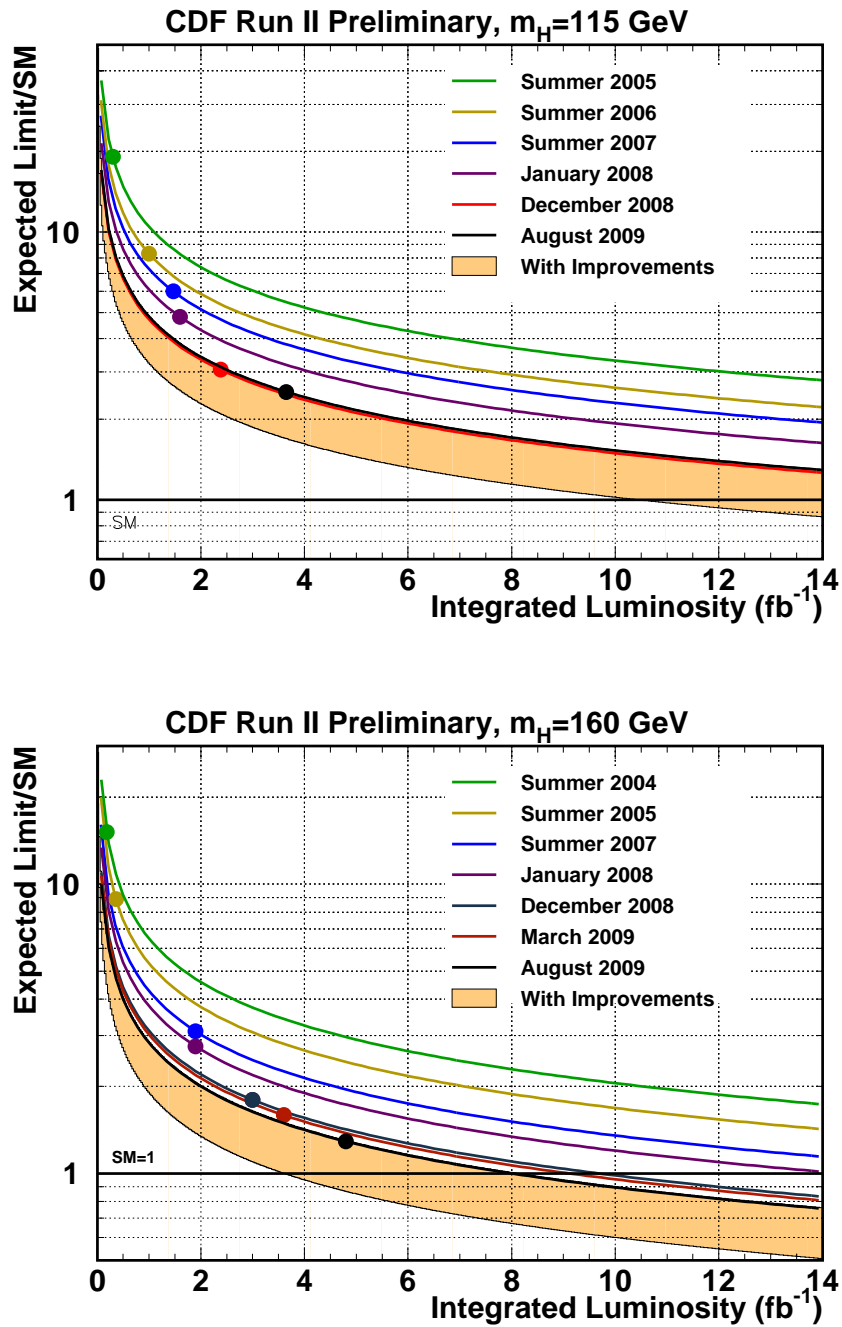


FIG. 8: Sensitivity projections and achieved sensitivities for the combined CDF Higgs boson searches, at  $m_H = 115$  and  $160$   $\text{GeV}/c^2$ . The curves are proportional to  $1/\sqrt{\int L dt}$  extrapolations of the median expected limits, and each analysis update corresponds to a new point with a new curve. The light orange bands indicate ranges of possible improvements in performance, relative to the Summer 2007 sensitivity. The top of the light orange bands is a factor of 1.5 below the Summer 2007 curve, and the bottom of the light orange bands are a further factor of 1.5 below the top of the light orange bands.

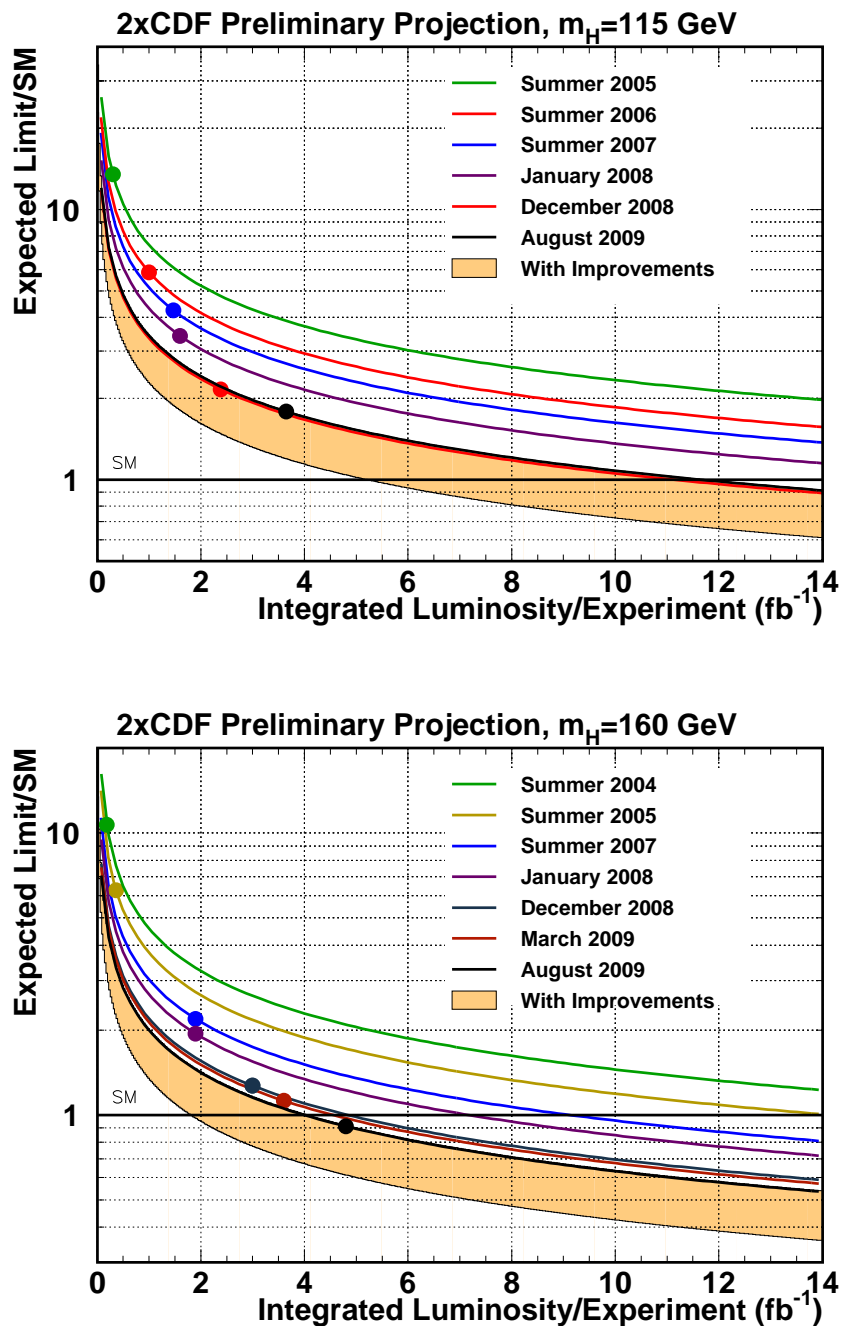


FIG. 9: Sensitivity projections and achieved sensitivities for the combined CDF Higgs boson searches, at  $m_H = 115$  and  $160$   $\text{GeV}/c^2$ , with a multiplier of  $1/\sqrt{2}$  applied to the expected limits, to approximate the contribution of D0, assuming identical performance. The curves are proportional to  $1/\sqrt{\int L dt}$  extrapolations of the median expected limits, and each analysis update corresponds to a new point with a new curve. The light orange bands indicate ranges of possible improvements in performance, relative to the Summer 2007 sensitivity. The top of the light orange bands is a factor of 1.5 below the Summer 2007 curve, and the bottom of the light orange bands are a further factor of 1.5 below the top of the light orange bands. The points represent CDF's achieved sensitivities, where the expected limits have been divided by  $\sqrt{2}$ .

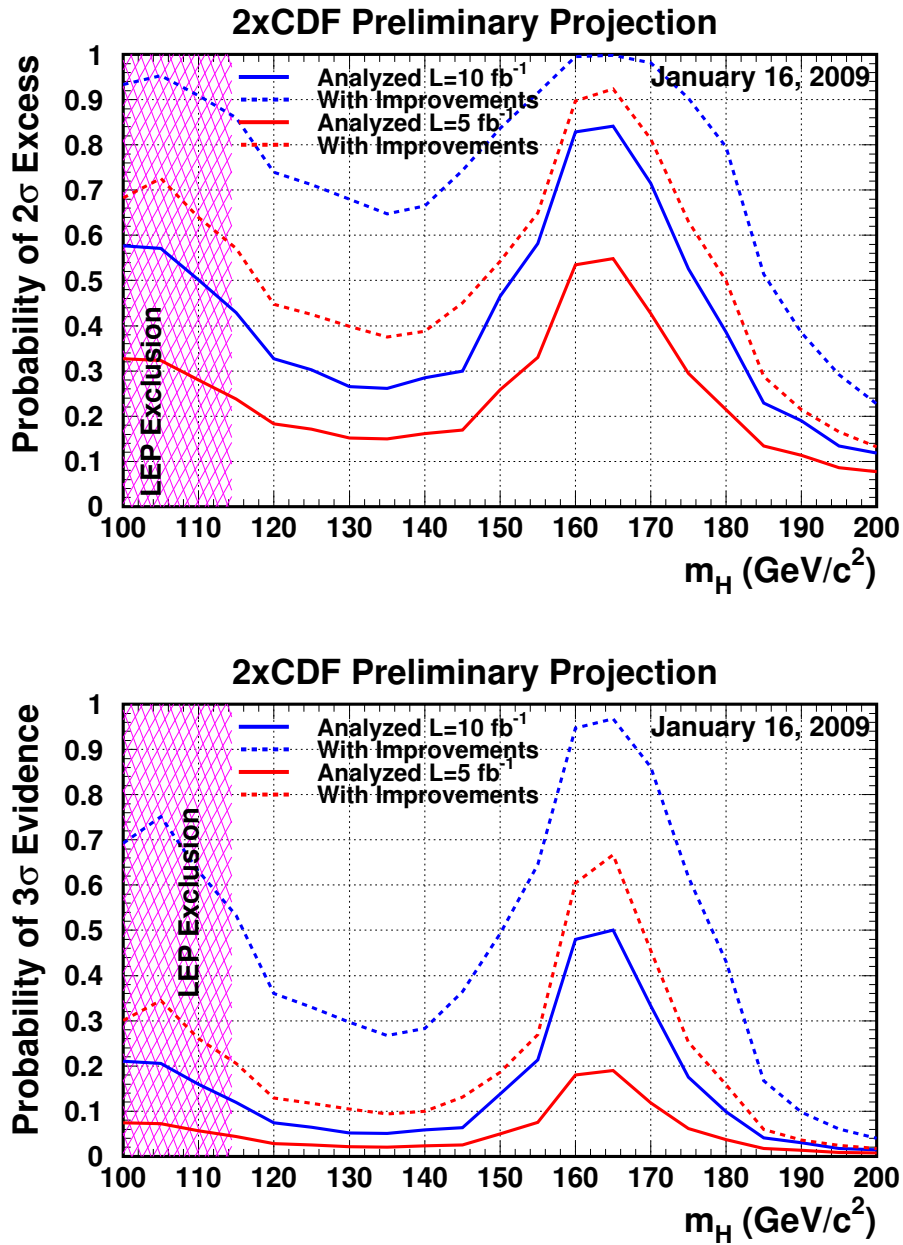


FIG. 10: Sensitivity projections as functions of  $m_H$ . These graphs show the chances of observing a  $2\sigma$  excess (top) or a  $3\sigma$  evidence (bottom), as functions of  $m_H$ , assuming a Higgs boson is present with production cross sections and decays at their SM values. CDF and D0 are assumed to contribute equally. The solid lines correspond to current performance as described in this note, and the dashed lines correspond to a performance level which corresponds to the bottom of the light orange bands in Figure 9. No account is taken of the data already collected and analyzed; existing excesses and deficits in the data do not affect these sensitivity projections. Two luminosity scenarios are considered:  $5 \text{ fb}^{-1}$  of analyzed luminosity per experiment (red lines) and  $10 \text{ fb}^{-1}$  of analyzed luminosity per experiment (blue lines).